2022

Extracellular vesicles and lipid flippase regulators in C. elegans

Lauren Pitts
University of Denver

Extracellular vesicles and lipid flippase regulators in C. elegans

Abstract

Extracellular vesicles (EVs) are membrane derived organelles released by all cell types and carry a vast array of cargos that can influence communication, development, and disease. One type of EV, known as microvesicles, form by budding directly from the plasma membrane in a process known as ectocytosis, however the mechanisms that govern this process are poorly understood. In C. elegans, the P4-ATPase, TAT-5, along with its activator, PAD-1, inhibit EV release from the plasma membrane by inhibiting phosphatidylethanolamine (PE) exposure on the outer leaflet of the plasma membrane. We identified 3 key domains of PAD-1 that are required to inhibit EV release and characterized alleles of TAT-5 and PAD-1, including a PAD-1 gain-of-function allele. These newly identified domains and characterized alleles provide us new opportunities to test the in vivo roles of TAT-5 and PAD-1, which in return will help us better understand the mechanisms that govern EV biogenesis.

Document Type

Thesis

Degree Name

M.S.

Department

Biological Sciences

First Advisor

Ann Wehman

Second Advisor

Joe Angleson

Third Advisor

J. Todd Blankenship

Keywords

Cells, Extracellular vesicles, Microvesicles, Ectocytosis

Subject Categories

Cell and Developmental Biology | Cell Biology | Life Sciences

Extracellular vesicles and lipid flippase regulators in *C. elegans*

A Thesis

Presented to

the Faculty of the College of Natural Sciences and Mathematics

University of Denver

In Partial Fulfillment

of the Requirements for the Degree

Master of Science

by

Lauren Pitts

August 2022

Advisor: Dr. Ann Wehman

Author: Lauren Pitts
Title: Extracellular vesicles and lipid flippase regulators in *C. elegans*
Advisor: Dr. Ann Wehman
Degree Date: August 2022

Abstract

Extracellular vesicles (EVs) are membrane derived organelles released by all cell types and carry a vast array of cargos that can influence communication, development, and disease. One type of EV, known as microvesicles, form by budding directly from the plasma membrane in a process known as ectocytosis, however the mechanisms that govern this process are poorly understood. In C. elegans, the P4-ATPase, TAT-5, along with its activator, PAD-1, inhibit EV release from the plasma membrane by inhibiting phosphatidylethanolamine (PE) exposure on the outer leaflet of the plasma membrane. We identified 3 key domains of PAD-1 that are required to inhibit EV release and characterized alleles of TAT-5 and PAD-1, including a PAD-1 gain-of-function allele. These newly identified domains and characterized alleles provide us new opportunities to test the *in vivo* roles of TAT-5 and PAD-1, which in return will help us better understand the mechanisms that govern EV biogenesis.

Table of Contents

List of Figures

Chapter One

Chapter Two

Chapter Three

Chapter Four

Chapter Five

List of Tables

Chapter Three

Chapter Seven

Author: Lauren Pitts
Title: Extracellular vesicles and lipid flippase regulators in *C. elegans*
Advisor: Dr. Ann Wehman
Degree Date: August 2022

Abstract

Extracellular vesicles (EVs) are membrane derived organelles released by all cell types and carry a vast array of cargos that can influence communication, development, and disease. One type of EV, known as microvesicles, form by budding directly from the plasma membrane in a process known as ectocytosis, however the mechanisms that govern this process are poorly understood. In C. elegans, the P4-ATPase, TAT-5, along with its activator, PAD-1, inhibit EV release from the plasma membrane by inhibiting phosphatidylethanolamine (PE) exposure on the outer leaflet of the plasma membrane. We identified 3 key domains of PAD-1 that are required to inhibit EV release and characterized alleles of TAT-5 and PAD-1, including a PAD-1 gain-of-function allele. These newly identified domains and characterized alleles provide us new opportunities to test the *in vivo* roles of TAT-5 and PAD-1, which in return will help us better understand the mechanisms that govern EV biogenesis.

Table of Contents

List of Figures

Chapter One

Chapter Two

Chapter Three

Chapter Four

Chapter Five

List of Tables

Chapter Three

Chapter Seven

Chapter 1: Introduction

1.1 Extracellular vesicles

Extracellular vesicles (EVs) are membrane-wrapped structures released by all prokaryotic and eukaryotic cells studied (Deatherage & Cookson, 2012; Schwechheimer & Kuehn, 2015; Cui et al., 2019; Gill et al., 2019). EVs are heterogeneous and contain different molecular cargos including nucleic acids, proteins, and lipids (Van Niel et al., 2018). EVs are involved in many physiological processes including communication, development, and behavior (Beer et al., 2017). For instance, in *C. elegans*, seam cells release EVs to properly build the alae (Liégeois et al., 2006). EVs are also released from *C.elegans* ciliated neurons to induce male mating behaviors (Wang et al., 2014), and *Drosophila* release EVs to reduce female remating behavior (Corrigan et al., 2014).

EVs are also found to play a role in pathological and clinical processes and have been implicated in many diseases, like cancer. For example, cancer cells have increased EVs that carry cargo that promote metastasis (Ciardiello et al., 2016). EVs extracted from human biofluids like blood, spinal fluid, or urine are used as clinical biomarkers that can provide invaluable information about a patient's disease state (Gong et al., 2015; Torrano et al., 2016; De Palma et al., 2016). EVs are also being developed as new drug delivery systems to deliver therapeutic agents to specific cells or tissue (El Andaloussi et al., 2013; Herrmann et al., 2021). EVs are similar to previously used delivery systems like

liposomes, as they both have membranes that are phospholipid based. However, unlike liposomes that are composed of artificial membranes, EV membranes are composed of lipids and membrane proteins that have closer membrane content to innate membranes (Mathieu et al., 2019; Ohno et al., 2016). These properties may allow EVs to deliver drugs more efficiently. For these reasons, understanding how EVs are produced and regulated can give great insight into both physiological and pathological processes.

1.2 Types of extracellular vesicles

Extracellular vesicles are separated into two subtypes known as exosomes and microvesicles. Exosomes are 30-100nm EVs that are derived from endosomes. Exosomes are formed through exocytosis, when multivesicular bodies (MVB) fuse with the plasma membrane and release internal intraluminal vesicles to the extracellular space (Beer et al., 2017). Internal intraluminal vesicles (ILVs) form from inward budding of the endosomal membrane (Beer et al., 2017) and MVBs are endosomes with multiple ILVs.

Microvesicles, also known as ectosomes, are formed through ectocytosis. Ectocytosis is the process of forming microvesicles by direct budding of the plasma membrane into the extracellular space (Beer et al., 2017). Microvesicles vary in size and are released in many diverse processes to create different microvesicle subtypes. For instance, 90–500 nm in diameter microvesicles are released during ectocytosis (Wehman et al., 2011), while midbodies and polar bodies are 1–3 μm vesicles that are released during asymmetric cytokinesis (Kalra et al., 2017; Beer et al., 2017; Li et al., 2013). Thus, extracellular vesicles are diverse structures that can range in size and origin.

1.3 ESCRT controls EV budding

The endosomal Sorting Complex Required for Transport (ESCRT) is one of the few known membrane-sculpting complexes to bend membranes away from the cytoplasm and are necessary for release of exosomes and microvesicles (Hurley et al., 2015). The ESCRT complex is divided into four subcomplexes including ESCRT-0, ESCRT-I, ESCRT-II and ESCRT-III. ESCRT-0 engages at the bud site and clusters ubiquitinated cargo, and recruits ESCRT-I and ESCRT-II. Meanwhile, ESCRT-I and ESCRT-II form membrane buds by curving membranes. Additionally, ESCRT-I and ESCRT-II recruit ESCRT-III which facilitates vesicle scission and release (Henne et al., 2011, Beer et al., 2017). Disassociation of ESCRT subcomplexes from the plasma membrane is facilitated by collapse of ESCRT-III coils by the disassembly factor VPS4 (Henne et al., 2013).

ESCRT plays a role in exosome biogenesis in worms and flies, similar to mammals (Colombo et al., 2014; Hurley et al., 2015; Abels et al., 2016; Beer et al., 2017). A screen in *C. elegans* identified 10 ESCRT proteins important for exosome biogenesis and alae formation (Hyenne et al., 2015). These proteins include ESCRT-0 subunit (HGRS-1), ESCRT-I subunits (TSG-101, VPS-28, VPS-37), ESCRT-II subunits (VPS-22, VPS-25, VPS-36), ESCRT-III subunits (VPS-20, VPS-32), and VPS-4. *Drosophila* ESCRT-0 subcomplex, Hrs, along with its accessory factor, ALiX, were found to be required for exosome secretion in male gland cells to inhibit female remating behavior (Corrigan et al., 2014; Van Niel et al., 2018; Tamai et al., 2010; Bai et al., 2021)

ESCRT also plays a conserved role in microvesicle release from the plasma membrane.

In mammals, ESCRT-1 subunits, TSG101 and VPS4, are required for microvesicle budding (Nabhan et al., 2012; Kalra et al., 2016). ESCRT proteins are also required for plasma membrane budding in *C. elegans* embryos. For example, ESCRT-I (TSG-101) and ESCRT-III (VPS-32) proteins were increased when microvesicle budding was increased and depleting ESCRT-0 (HGRS-1, STAM-1) or ESCRT-I (TSG-101, VPS-28) subcomplexes suppressed microvesicle release in *C. elegans* embryos (Wehman et al., 2011).

Thus, ESCRT complexes play a role in both exosome and microvesicle release. However, in order to understand the *in vivo* functions of EVs we must be able to differentiate between EV subgroups. Therefore, we should look at other regulators of EV release that are unique to microvesicles or exosomes.

1.4 Loss of phosphatidylethanolamine asymmetry results in a higher yield of EVs released

The phospholipid bilayer of plasma membranes is a key structure that defines cells and organelles (Timcenko et al., 2019). Maintaining phospholipid asymmetry is important for many cellular processes including cell fusion, division, and death (Wehman et al., 2011; Emoto et al., 1996; Emoto & Umeda, 2000; Emoto et al., 1997; Irie et al., 2017). Maintaining phosphatidylethanolamine (PE) asymmetry is important for regulating extracellular vesicle release. Previous work has found an increase in EVs from

the plasma membrane when cytofacial PE is externalized on the outer leaflet of the plasma membrane in *C. elegans* embryos (Wehman et al., 2011). PE is also found to be externalized on the surface of human derived EVs (Larson et al., 2012), suggesting that PE may play an important role in EV formation.

Phospholipid asymmetry is maintained and regulated by lipid transporters known as scramblases, floppases, and flippases. Scramblases are bidirectional lipid transporters that disrupt phospholipid distribution in an ATP-independent manner (Sahu, Gummadi, Manoj, & Aradhyam, 2007). For example, in humans with Scott syndrome, mutations of TMEM16F scramblase disrupts PS and PE externalization and reduce EV release (Suzuki et al., 2010; Castoldi et al., 2011). The second type of transporters are floppases. Floppases are ATP Binding Cassette (ABC) that transport phospholipids to the extracellular leaflet of the plasma membrane (Zwaal et al., 2005; Leventis & Grinstein, 2010; Rees et al., 2009).

Lastly, a third type of lipid transporter is known as a flippase. Flippases are ATP-dependent transmembrane proteins that translocate phospholipids from the outer leaflet of the plasma membrane to the inner leaflet (Zwaal et al., 2005; Leventis & Grinstein, 2010). Flippases have been shown to function in EV regulation. For example, the PE flippase activity of TAT-5 has been found to inhibit EV budding from the plasma membrane in *C. elegans* (Wehman et al., 2011).

1.5 P4-ATPases

Flippases are part of the P-type ATPase family that transport substrates across biological membranes by forming ATP-dependent phosphorylated intermediates (Axelsen & Palmgren 1998). P-Type ATPases include five subclasses, P1 through P5, that transport a diverse range of substrates. The first three classes mainly transport cations or heavy metals, while P4-ATPases transport phospholipids (Bai et al., 2021; Palmgren et al., 2019). The last subclass, P5 ATPases, transport transmembrane helices or polyamines across lipid bilayers (Feng et al., 2020; McKenna et al., 2020).

P-type ATPases are made up of a transmembrane domain (TMD), an actuator domain (A-domain), a nucleotide-binding domain (N-domain), and a phosphorylation domain (P-domain) (Bai et al., 2021; Palmgren & Nissen 2011). P-Type ATPases transport their substrates through an ATPase catalytic cycle known as the Post-Albers cycle (Andersen et al., 2016). This cycle starts with the E1 state when ATP and a substrate bind, and then moves into the E1P state after autophosphorylation (Andersen et al., 2016; Bai et al., 2021). Next, the movement of the P domain moves the TM domain 3 and A domain to the E2P state. The A domain then facilitates dephosphorylation of the E2P to E2 state where the substrate is transported and the A domain returns to its original position so the cycle can start again (Lopez-Marques et al., 2020; Bai et al., 2021)

P4-ATPases are conserved in eukaryotes such as yeast, mammals, and *C. elegans* (van der Mark et al., 2013). Yeast such as *Saccharomyces cerevisiae* has five P4 ATPases: Drs2, Neo1, Dnf1, Dnf2, and Dnf3 (Bai et al., 2021). Mammals have fourteen P4-ATPases that include ATP8A1-2, ATP8B1-4, ATP9A-B, ATP10A-D, and ATP11A-

C (Bai et al., 2021; Shin & Takatsu, 2018). *C. elegans* have six P4-ATPases which include TAT-1-6 (Lyssenko et al., 2008). These different P4-ATPases have different substrate specificity (ie. PC, PS, and PE) and localization (Bai et al., 2021).

Most P4-ATPases transport phospholipids with the help of a β-subunit to form a heterodimeric complex, where the β-subunit is a partner protein and the α- subunit is the major catalytic subunit (Bai et al., 2021). The β-subunit is essential for P4-ATPase localization outside of the ER and flippase activity. However, no β-subunit or cofactor has been identified in yeast Neo1, or its *C. elegans* or human orthologs, TAT-5 and ATP9A or B so far.

1.6 *C. elegans* as a genetic model organism for extracellular vesicle release

To research the *in vivo* functions of EVs we used *Caenorhabditis elegans* as the model organism. *C. elegans* has a rapid life cycle of just three days from embryo to egg-laying (Corsi et al., 2015), which allows us to easily study every step of development. *C. elegans* are also transparent and their embryogenesis follows a defined pattern of cell division that can easily be followed *in vivo* using time-lapse microscopy (Sulston et al., 1983). Genetic approaches like transgenesis, knock out, and knockdown are well established in *C. elegans* (Boulin & Hobert, 2012), and can allow us to study molecular functions *in vivo*. Additionally, many genes in *C. elegans* have functional orthologs in humans, which makes *C. elegans* a practical model to study human diseases (Corsi et al., 2015). Furthermore, *C. elegans* are cost efficient and lack any ethical conflicts of studying their embryos, making them the ideal model organism for our study.

1.7 Labeling and quantifying EVs using degron tags

In order to study the *in vivo* functions of EVs, we must be able to label specific subtypes of EVs. In our study, we use degron-tagged reporters to label and visualize microvesicles released from the plasma membrane. Degrons are small degradation motifs that target specific proteins for ubiquitination and degradation (Beer et al., 2019). Degrons recruit cytosolic ubiquitin ligases in order to polyubiquitinate target proteins (Beer et al., 2019; Foot et al., 2017).

To study the release of microvesicles, degrons are tagged to the Plekstrin homology (PH) domain of the cytosolic phospholipase C (PLC) (Beer et al., 2019). PLC binds to PI4,5P2-containing membranes, including the plasma membrane (Kume et al., 2016) and therefore is able to label EVs. Once an EV is released into an extracellular space, degron tags are not accessible to ubiquitin ligases and are not degraded (Figure 1).

To study EV release in *C. elegans,* we used zinc finger 1 (ZF1) degron from the PIE-1 protein and C-terminal phosphodegrons (CTPD) degron from the OMA-1 protein. ZIF-1 is expressed in a stereotypical pattern of somatic cells and is not expressed in all cells such as the posterior germ cells (DeRenzo et al., 2003). Therefore, ZF1 degron tags are not degraded until after the 4-cell stage (Beer et al., 2021). OMA-1 on the other hand is expressed in maternally and inherited by all embryonic cells, and CTPD degron tags are degraded after the first cell division (Nishi et al., 2005; Beer et al., 2019). Therefore, by using these degron tags we are able to label and quantify EVs released directly from the plasma membrane in various embryo stages.

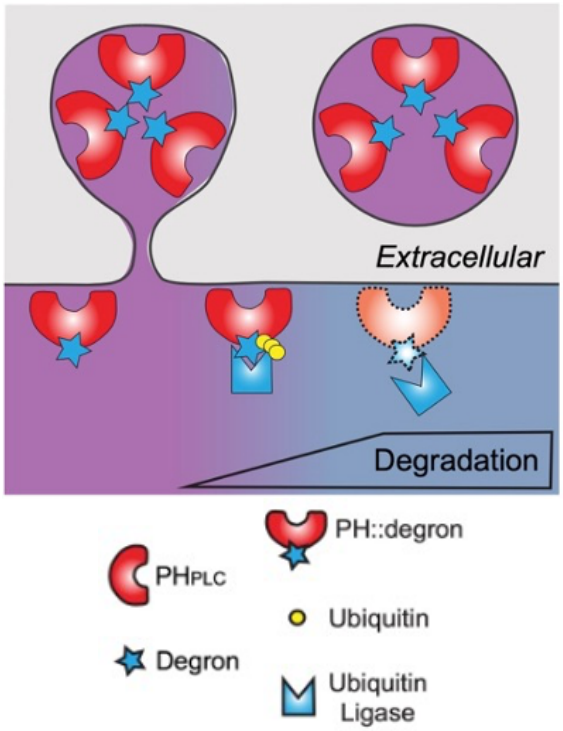

Figure 1. Using degron tags to label extracellular vesicles
The degrons tagged to the PH domain of PLC are recognized by ubiquitin ligase. Polyubiquitination of degron reporter leads to loss of tagged fluorescent reporters shown by the dotted lines. Degron tags released in microvesicles are not accessible to ubiquitin ligases and are not degraded. *Reproduced from Beer et al., Nature Communications, 2019*

1.8 TAT-5 and its activator PAD-1 inhibit extracellular vesicle release in *C. elegans*

TAT-5 is a phospholipid flippase that maintains PE asymmetry in the plasma membrane and inhibits ESCRT-mediated ectocytosis in *C. elegans* (Wehman et al., 2011). When TAT-5's function or localization is lost, PE, which is normally located on the cytosolic leaflet of the plasma membrane, is externalized and an overproduction of EVs occurs (Wehman et al., 2011). These observations show that TAT-5 is a key regulator of extracellular release in *C. elegans*, and therefore is a key interest of study for understanding the regulation of EVs.

The Dopey protein PAD-1 has been shown to be an upstream activator of TAT-5 and inhibits extracellular release without disrupting TAT-5 localization (Beer et al., 2018). For example, when *pad-1* is knocked down via RNAi, an increase in EV release similar to loss of TAT-5 is observed (Beer et al., 2018). Deletion of *pad-1* was also found to cause sterility and embryonic lethality, but not did not disrupt TAT-5 localization (Beer et al., 2018). Together these results show that PAD-1 is needed for TAT-5 activity and indirectly regulates EV release by TAT-5.

Loss of TAT-5 and PAD-1 lead to similar phenotypes including: sterility, embryonic lethality, increased EV release, and MVB morphological defects. Loss of TAT-5 and PAD-1 can also disrupt phagocytosis of midbody remnants and polar bodies (Fazeli et al., 2020). Midbody remnants are extracellular vesicles formed and released at the end of cell divisions (Fazeli et al., 2016), while polar bodies are cell corpses formed and released during female meiosis (Fabritius et al., 2011). However, it is unclear whether TAT-5 and PAD-1 disrupt phagocytosis by externalizing PE or if it is disrupted by increased EV accumulation between cells.

Together these phenotypes show the importance of TAT-5 and EV regulation, however, there is still much to learn about how this pathway is regulated. Thus, it is the goal of this thesis to further characterize the mechanisms that govern TAT-5 and PAD-1, which in return will help us better understand the mechanisms that control EVs.

Chapter Two: Characterizing EV release in *tat-5* and *pad-1* mutants

2.1 Introduction

To better understand the *in vivo* functions of EVs we must understand how they are regulated. Previous studies by our lab have found that disrupting TAT-5 and PAD-1 can lead to many severe loss of function phenotypes including sterility, embryonic lethality, increased EV release, enlarged multivesicular bodies, and phagocytosis defects of both cell debris and cell corpses (Wehman et al., 2011; Beer et al., 2018; Fazeli et al., 2020). However partial disruption of functional PAD-1 alleles like GFP::PAD-1 are fertile and viable and have moderate loss of function phenotypes such as mild increase in EV release and only disrupt phagocytosis of debris (midbody remnants) (Beer et al. 2018; Fazeli et al., 2020). By identifying and scoring for these phenotypes in modified PAD-1 and TAT-5 alleles we can identify if point mutations or fluorescent knock-ins affect PAD-1 and/or TAT-5 function.

Previous studies have also quantified the number of EVs released in embryos by using mCh::PH::ZF1 degron tags that label EVs released from the plasma membrane (Fazeli et al., 2020; Beer et al., 2019). ZF1 degron tags are degraded in a stereotyped pattern of somatic cells, starting with the anterior cells (Beer et al., 2019). ZF1 degron tags are also not degraded until after the four-cell stage in somatic cells and are not degraded in cells that do not express ZIF-1, such as posterior germ cells (Beer et al.,

2019). This makes it difficult to distinguish individual EVs in early embryos, as the neighboring plasma membrane is bright. mCh::PH::CTPD degron tags, however, begin to be degraded after the first cell division (Beer et al., 2019). Therefore, mCh::PH::CTPD degron tags can be used to quantify EVs released in early embryos.

Thus, the goal of this chapter is to use known loss-of-function phenotypes to characterize TAT-5 and PAD-1 fluorescent knock-in and point mutation alleles and further quantify EV release in TAT-5 and PAD-1 mutants using mCh::PH::CTPD degron tag.

2.2 Results

2.2.1 Scoring sterility and embryonic lethality in TAT-5 and PAD-1 knock-in and point mutations

To further our understanding of TAT-5 and PAD-1, we created *tat-5* and *pad-1* point mutation and fluorescent knock-in mutants using CRISPR/Cas9-mediated genome editing and scored for viable progeny (Paix et al., 2014). To test the roles of TAT-5 nucleotide binding domain (N domain) we mutated Phenylalanine 570 to alanine (F570A) in the N-domain of TAT-5. Conserved F570 has been shown to interact with ATP in the N domain of both yeast and human P4-ATPases (Hiraizumi et al., 2019; Timcenko et al., 2019). Previous studies by our lab found that GFP::TAT-5(F570A) transgenes did not rescue sterility phenotypes in *tat-5* mutants, which suggested that GFP::TAT-5(F570A) may not be a functional TAT-5 allele (Causemann, 2019). Therefore, we predicted that the CRISPR *tat-5(F570A)* mutant would be sterile. Julia Frondoni scored for viable progeny and found that *tat-5(F570A)* mutants are fertile but

have a 1.4 fold decrease in progeny compared to wild type control ($p<0.01$, Figure 2.1). These data suggest that *tat-5(F570A)* is a partial loss of function allele.

To identify additional loss-of-function alleles of TAT-5, we next mutated Lysine 1059 (K1059) to Arginine. K1059 corresponds to lysine 1224 (K1224) in Drs2p, and studies have shown that the yeast P4-ATPase Drs2p is activated after the binding of PI4P to a pocket made by three transmembrane domains and the C-terminus, including K1224 in the tenth transmembrane domain (Timcenko et al., 2019). Previous studies by our lab found that transgenes expressing *tat-5(K1059R)* only partially rescued growth when crossed with *tat-5* deletion mutants, which suggested that they were partially non-functional (Causemann, 2019). Therefore, we predicted that TAT-5(K1059R) would be slow growing or have reduced progeny. Indeed, upon generating the strain, SunyBiotech reported that the strain was slow growing, taking 2 days longer than normal to grow. Julia Frondoni in our lab found that *tat-5(K1059R)* mutants have a 1.6 fold reduction in progeny compared to wild type control ($p<0.05$, Figure 2.1). This data suggests that *tat-5(K1059R)* is also a partial loss of function *tat-5* allele.

Additionally, we mutated TAT-5's lysine 1064 (K1064) to Arginine to study the roles of the conserved C-terminal lysines, which are possible targets of ubiquitination. Previous studies by our lab found that mutants expressing GFP::TAT-5(K1059R K1064R K1072R) transgenes (abbreviated KKKRRR) had significantly more plasma membrane intensity compared to the control, suggesting that GFP::TAT-5(KKKRRR) could disrupt ubiquitin-mediated endocytosis of TAT-5 (Causemann, 2019). GFP::TAT-5(KKKRRR) transgenes were also unable to rescue sterility in a *tat-5* deletion background, suggesting

that either the lysine in TM10 or the C-terminal lysine residues were required for TAT-5 function (Causemann, 2019). Therefore, we wanted to test the effect of *tat-5(K1064R)* or *tat-5(K1064R K1072R)* mutants on sterility and embryonic lethality. However, Julia Frondoni in our lab found that both *tat-5(K1064R)* and *tat-5(K1064R K1072R)* mutants were fertile and did not significantly differ in the number of progeny from wildtype control ($p>0.05$, Figure 2.1). These data suggest that K1064 and K1072R are not required for the essential functions of TAT-5.

To test the roles of TAT-5's actuator domain (A domain), we mutated Aspartic acid 244 (D244) to Threonine. Mutations equivalent to D244T in the DGET motif in the A domain of the human P4-ATPase ATP8A2 led to a 3-fold decrease in lipid transport and ATPase activity (Coleman et al., 2012). As deletion of *tat-5* causes sterility, while RNAi knockdown causes embryonic lethality (Wehman et al., 2011), we hypothesized that TAT-5(D244T) could cause sterility or embryonic lethality. Julia Frondoni in our lab found that *tat-5(D244T)* mutants were not sterile, with an average of 77 ±43 embryos, but caused embryonic lethality ($p<0.001$, Figure 2.1). Together, this data suggests that *tat-5(D244T)* is a strong loss-of-function allele but not a null allele.

Glutamate E198 in the human P4-ATPase ATP8A2 has been shown to be an essential residue for ATPase activity. For instance, one study found that ATP8A2(E198Q) mutants did not have detectable ATPase activity (Coleman et al., 2012). Previous studies by our lab also found that mutants expressing a GFP::TAT-5(E246Q) transgene, corresponding to E198Q in ATP8A2, failed to rescue the sterility and maternal-effect embryonic lethality of *tat-5* deletion mutants (Wehman et al., 2011).

These data suggested that E246 is similarly essential for TAT-5 activity. To confirm these findings, we again used CRISPR to mutate Glutamic acid 246 (E246) to Glutamine in TAT-5. Julia Frondoni found that *tat-5(E246Q)* mutants were mostly sterile and only had an average of 0.5±1 embryos, which died during embryogenesis. This data suggests that *tat-5(E246Q)* is a null TAT-5 allele.

We also created *tat-5* and *pad-1* fluorescent knock-in mutations that include GFP knocked into the N-terminus of TAT-5 (GFP::TAT-5), GFP knocked into the N-terminus of PAD-1 (GFP::PAD-1), mScarlet knocked into the C-terminus of PAD-1 (PAD-1::mScarlet), and mScarlet-I knocked into the C-terminus of PAD-1 (PAD-1::mScarlet-I). We found that all fluorescent knock-in mutants were viable and did not have a significantly different number of progeny from wildtype control ($p>0.05$, Figure 2.1). These data suggest that these fluorescent knock-ins are at least partially functional *tat-5* and *pad-1* alleles.

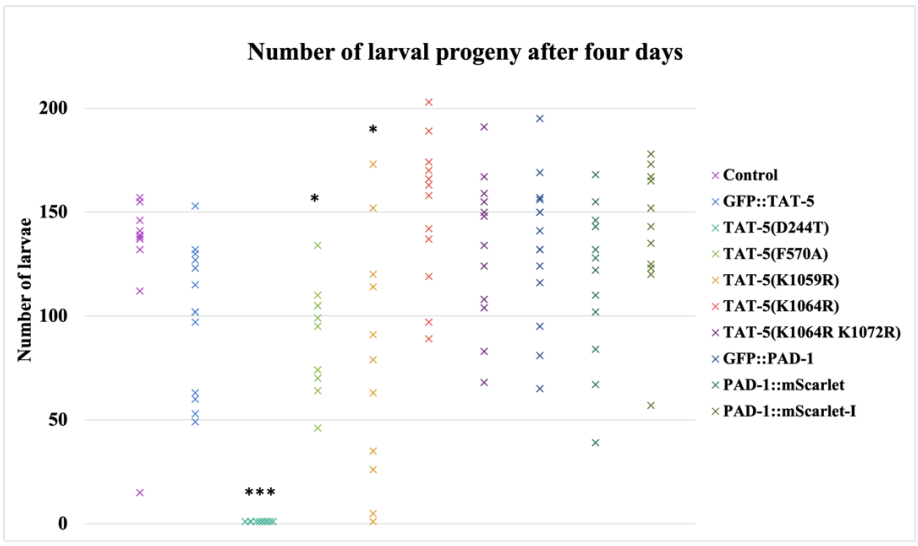

Figure 2.1. Most PAD-1 and TAT-5 knock-in or point mutant alleles are viable and fertile

Only TAT-5(D244T) results in embryonic lethality. Each data point represents the number of larval progeny that were scored 4 days after singling one hermaphrodite worm. Scoring for larval progeny from TAT-5(D244T), TAT-5(F570A), TAT-5(K1059R), TAT-5(K1064R), and TAT-5(K1064R K1072R) was done by Julia Frondoni. Mutant alleles compared to control using Student's t-test with Bonferroni correction. *$p<0.05$, ***$p<0.001$ compared to control.

2.2.2 Scoring EV release in TAT-5 and PAD-1 knock-in and point mutations

We next examined EV release in TAT-5 and PAD-1 knock-in and point mutations using mCh::PH::CTPD degron tag to label EVs released directly from the plasma membrane (Beer et al., 2019). As an increase in EV release disrupts gastrulation and results in embryonic lethality, and ATPase activity is required for TAT-5 to inhibit EV release (Wehman et al., 2011), we expected that the predicted ATPase hypomorph *tat-5(D244T)* mutants that causes embryonic lethality would also cause an increase in EV release. We found that TAT-5(D244T) does cause a 100-fold increase in EV release with

an average of 134±63 EV puncta (Figure 2.2 D). This data supports our hypothesis and further suggests that TAT-5(D244T) is a strong loss of function allele.

We found that EV release in GFP::TAT-5, PAD-1::mScarlet, and PAD-1::mScarlet-I, as well as *tat-5(F570A)* and *tat-5(K1059R)* mutants did not cause a significant difference in EV release compared to wildtype control ($p>0.1$, Figure 2.2 D). These data suggest that these fluorescent knock-in and point mutations do not disrupt TAT-5 or PAD-1 ability to regulate EVs.

We did see a significant increase in EV release in GFP::PAD-1 mutants compared to wildtype control ($p<0.001$, Figure 2.2 D). However, GFP::PAD-1 only caused a 20-fold increase in EVs with an average of 20±16 EV puncta (Figure 2.2 D), similar to EV results found while using PH::ZF1 degron reporter (Fazeli et al., 2020). These results further suggest that knock-in of GFP into the N-terminus of PAD-1 is only partially disrupting PAD-1 function.

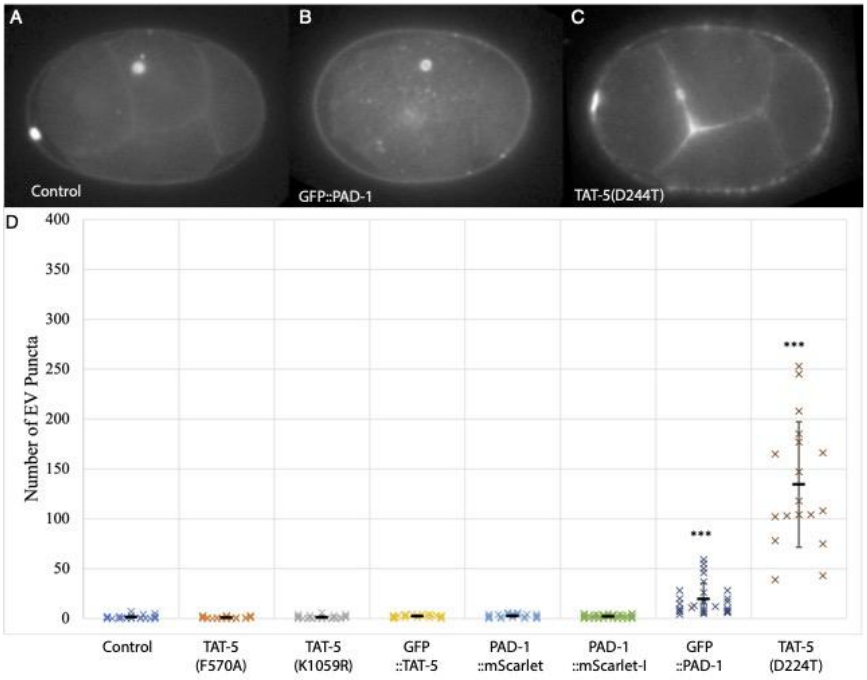

Figure 2.2. Screening EV release in PAD-1 and TAT-5 knock-in or point mutant alleles

A-C: 4-cell embryos expressing mCh::PH::CTPD in control (A) GFP::PAD-1 (B) and TAT-5(D244T) (C).

D: The number of mCh::PH::CTPD EV puncta inside the eggshell of tat-5(K1059R), tat-5(F570A), GFP::TAT-5, PAD-1::mScarlet, and PAD-1::mScarlet-I mutant embryos is not significantly different from control embryos ($p>0.05$). GFP::PAD-1 partially disrupts PAD-1 function, resulting in a mild but significantly different increase in EV release (***$p<0.001$). The TAT-5(D244T) allele with reduced ATPase activity results in a severe increase in EV release compared to control (***$p<0.001$). Each data point represents the number of EV puncta observed in a single embryo. Mutants compared using Student's t-test with Bonferroni correction. Mean ± S.D. shown.

2.2.3 Severe increased EV release disrupts phagocytosis of second polar bodies

We next investigated loss of function phenotypes seen with severe increases in EV release, such as polar body phagocytosis. To test this, we again used mCh::PH::CTPD degron tag to label polar bodies, as CTPD degradation does not occur inside polar bodies (Beer et al., 2019). We scored for second polar body (2PB)

internalization in our TAT-5 and PAD-1 knockin and point mutation mutants and found that all mutants, except for ATPase hypomorph *tat-5(D244T)* ($p<0.01$, Figure 2.3), internalized 2PB ($p>0.1$, Figure 2.3). These results demonstrate that the majority of *tat-5* and *pad-1* knockin and point mutations do not have severe phagocytosis loss-of-function phenotypes. These findings are also consistent with observations seen with ZF1 degron tag in a *pad-1* partial loss of function allele and *tat-5* or *pad-1* knockdown (Fazeli et al., 2020) and further confirm *tat-5(D244T)* as a loss of function allele.

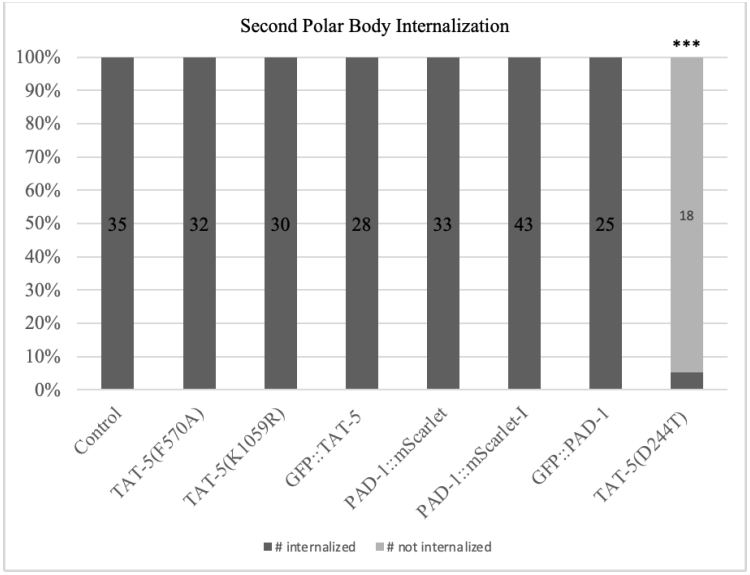

Figure 2.3. Severe increase in EVs disrupts polar body phagocytosis
Second polar bodies tagged with mCh::PH::CTPD were scored for internalization. Only TAT-5(D244T) disrupted polar body uptake by phagocytosis. Mutants compared using Fisher's exact test with Bonferroni correction, ***$p<0.001$ compared to control.

2.2.4 Mild increase in EV release disrupts phagocytosis of midbody remnants

Having established severe loss-of-function phenotypes like increased EV release and 2PB phagocytosis defects, we next investigated partial-loss-of function phenotypes, such as disrupted phagocytosis of midbody remnants (Fazeli et al., 2016). To test this, we crossed GFP::TAT-5, PAD-1::mScarlet, PAD-1::mScarlet-I, and *tat-5(D244T*) mutants with fluorescently-tagged non-muscle myosin, NMY-2.

We found GFP::TAT-5 and PAD-1::mScarlet internalized all P0 midbody remnants and therefore do not affect midbody remnant phagocytosis ($p>0.1$, Figure 2.4). PAD-1::mScarlet-I internalized all midbody remnants, except for 1. However, this was not found to be statistically different from the control ($p>0.1$, Figure 2.4), and suggest that PAD-1::mScarlet-I does not disrupt midbody remnant phagocytosis.

ATPase hypomorph *tat-5(D244T)* does significantly disrupt midbody phagocytosis compared to the control ($p<0.01$, Figure 2.4) and further suggests that TAT-5(D224T) is a loss-of-function allele.

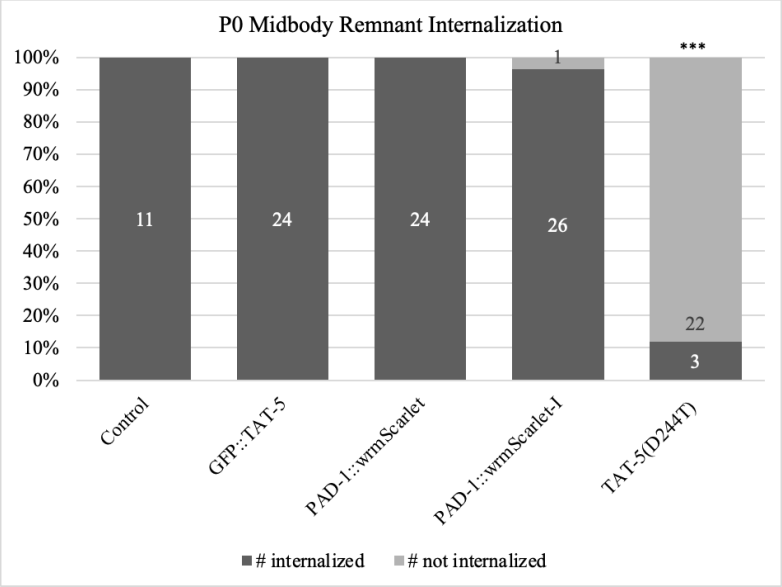

Figure 2.4. Mild increase in EV release disrupts midbody remnant phagocytosis P0 midbody remnants tagged with a NMY-2 fluorescent reporter were scored for internalization. TAT-5(D244T) disrupted midbody internalization. Mutants compared using Fisher's exact test with Bonferroni correction (***$p<0.001$ compared to control). Control data is from Fazeli et al., 2020.

2.3 Discussion

By screening previously identified TAT-5 and PAD-1 loss-of-function phenotypes, we determined that TAT-5 point mutations *tat-5(F570A)* and *tat-5(K1059R)* are fertile and do not increase extracellular vesicle release or disrupt phagocytosis but do have significantly fewer progeny. Together these data suggest that *tat-5(F570A)* and *tat-5(K1059R)* are partial loss of function TAT-5 alleles.

The hypomorphic ATPase TAT-5(D244T) allele was found to have severe loss-of-function phenotypes including embryonic lethality, increased EV release, and phagocytosis defects of both cell debris and cell corpses. However, they do appear to be more fertile and lay more embryos than *tat-5(E246Q)* mutants, suggesting that D244T is

not a complete loss of function allele. These results suggest that TAT-5(D244T) is a strong loss-of-function allele and further suggest TAT-5 flippase activity is required for EV regulation.

In previous studies, GFP::PAD-1 has been characterized as a partial loss-of-function allele, with disrupted cell debris phagocytosis and >20-fold increase in EV release (Beer et al., 2018; Fazeli et al., 2020). Our results confirm these findings, as we observed GFP::PAD-1 significantly disrupted midbody remnant phagocytosis, and caused a significant increase in EV release with an >20-fold increase in EV puncta. Due to this mild increase in EV release, GFP::PAD-1 can be used to score for increases or decreases in EV release, making GFP::PAD-1 a great candidate to use in enhancer/suppressor RNAi screens to identify either positive or negative EV regulators.

TAT-5 and PAD-1 fluorescent knock-in GFP::TAT-5, PAD-1::mScarlet, and PAD-1::mScarlet-I alleles are also viable and do not disrupt EV release or phagocytosis. While GFP::PAD-1 does appear to disrupt EV release and midbody phagocytosis (Fazeli et al., 2020). Together, these results suggest that fluorescent proteins inserted into the C-term of PAD-1 and N-term of TAT-5 do not disrupt EV regulation and therefore can be used to study TAT-5 and PAD-1 function and localization.

As increased EV release can be used to differentiate between severe or partial loss of function TAT-5 and PAD-1 alleles, it is important to accurately quantify the number of EVs released in embryos. However, counting EV puncta by eye can be quite taxing and time consuming, especially in mutants like *tat-5(D244T)* that can have hundreds of EV puncta. Counting EV puncta by eye can also lead to variability and human error. For

instance, one person may count a large EV puncta as two, while another individual counts the same large EV puncta as one or three. Therefore, an important next step to this study is to develop an automated system to count EV puncta in embryos.

Chapter Three: RNAi screen to identify TAT-5 cofactors

3.1 Introduction

Loss of TAT-5 activity increases PE externalization and extracellular vesicle (EV) release (Wehman et al., 2011). Maintaining phospholipid asymmetry and regulating EV release is important for many cellular processes including cell fusion, division, and death (Emoto et al., 1996; Emoto & Umeda, 2000; Emoto et al., 1997; Irie et al., 2017). Therefore, it is important to understand how the lipid flippase TAT-5 is regulated.

Most P4-ATPases require an accessory β-subunit such as cell division cycle protein 50 (CDC50) or ligand effect modulator 3 (LEM3) for proper exit out of the endoplasmic reticulum (ER) and flippase function (Bai et al., 2020; Andersen et al., 2016; Saito et al., 2004). CDC50 proteins are small proteins consisting of two TM domains and a large exoplasmic domain stabilized by disulfide bonds (Bryde et al., 2010). When CDC50 is lost in yeast and mammals, non-essential P4-ATPases fail to exit the ER and lose flippase function (Saito et al., 2004; van der Velden et al., 2010). Essential P4-ATPases like TAT-5 and its orthologs in yeast and mammals, however, do not require CDC50 proteins to exit the ER or for their flippase activity (Barbosa et al., 2010, Bai et al., 2021, Beer et al., 2018). For instance, in *C. elegans* double knockdown of CDC50 family proteins W03G11.2 and F20C5.4 in *chat-1* mutant background did not disrupt EV release or TAT-5 exit from the ER (Beer et al., 2018). These data suggest that

TAT-5 does not require CDC50 family proteins to properly localize to the plasma membrane and flip PE, however if TAT-5 requires other potential cofactors is unknown.

The Dopey protein PAD-1 has been shown to be an activator of TAT-5 and is required for TAT-5 flippase activity (Beer et al., 2018). However, PAD-1 is not required for TAT-5 localization out of the ER as TAT-5 was still able to localize to the plasma membrane in *pad-1* deletion embryos (Beer et al., 2018). PAD-1 is thought to regulate TAT-5 PE flipping activity through a different mechanism than CDC50, as PAD-1 does not share any sequence homology with CDC50 family proteins (Beer, 2021).

3.2 Results

3.2.1 Screening for potential TAT-5 interactors

To find potential cofactors or chaperones of TAT-5, a membrane split-ubiquitin yeast two-hybrid (MBMate Y2H) was performed by Hybrigenics to detect protein interactions in live yeast cells. In Y2H screens, the target protein, in our case TAT-5, is used as a bait to screen yeast libraries for preys made up of proteins found in *C. elegans* (Legrain & Selig, 2000). The MBMate Y2H screen yielded 77 potential TAT-5 interactors, 21 of these potential interactors were classified as transmembrane proteins with extracellular domains by an undergraduate member in our lab, Abran Bartlett-Miller (Table 3.1). We hypothesized that the 21 transmembrane proteins with an extracellular domain are most likely to be cofactors of TAT-5 as they have similar topology as CDC50 proteins.

Table 3.1: Transmembrane proteins with extracellular domains identified by MBMate Y2H

MBMate Y2H performed by Hybrigenics using TAT-5 as bait. The name, protein classification, and PBS confidence score are indicated. PBS confident scores identify protein interactions and potential false positives from A to D. A being most confident and D being least confident. Identified interactors were classified by Abran Bartlett-Miller.

Gene Name	Global PBS	Gene description
use-1	D	Membrane fusion protein Use1 and Vesicle transport protein, Use1
pyp-1	D	Inorganic diphosphatase activity and magnesium ion binding activity. In innate immune response.
F01G4.6	D	Mitochondrial carrier protein. Ortholog of human SLC25A3
acl-14	D	Ortholog of human LPGAT1. Transferase activity for acyl groups.
nbet-1	B	Target SNARE coiled-coil homology domain and BET1-like protein.
atln-1	D	GTP binding activity and GTPase activity. Involved in IRE1-mediated unfolded protein response.
ceh-44	D	DNA binding activity.
col-14	D	Collagen. Structural constituent of cuticle.
sdz-27	D	Involved in gastrulation.
Y41E3.8	D	In IRE1-mediated unfolded protein response.
F17E9.4	D	Protein of unknown function (DUF870)
ced-1	D	Scavenger receptor activity in cytoskeleton organization; left/right axis specification; and phagocytosis.
F57C2.4	D	In cephalic sheath cell; dopaminergic neurons; excretory cell; germ line; and hypodermis
C14B1.2	D	In BAG; germ line; germline precursor cell; intestine; and pharyngeal muscle cell

C44B7.5	D	In cephalic sheath cell; dopaminergic neurons; germ line; and hypodermis
F55G1.15	D	In GABAergic neurons; excretory cell; head mesodermal cell; and intestine
B0348.2	D	LITAF-like zinc ribbon domain; LPS-induced tumour necrosis factor alpha factor; and LITAF domain containing protein
Y34F4.2	B	Tight junction protein, claudin-like.
W02D9.6	D	In AVK
T07H8.11	D	Affected by xbp-1 based on RNA-seq studies.
ZK1290.13	D	In ASER; head mesodermal cell; and intestine.

3.2.2 Identifying potential TAT-5 and EV regulators

To better understand how TAT-5 activity is regulated to inhibit EV release, we performed an RNA interference (RNAi) screen targeting 19 of the 21 transmembrane proteins with extracellular domains. Only 19 of the 21 proteins were screened as two proteins (ATLN-1 and T07H8.11) do not have clones in available RNAi libraries. We scored for RNAi that caused a significant difference in EV release using mCh::PH::CTPD degron tag to label plasma membrane derived EVs (Beer et al., 2019). RNAi was performed on GFP::PAD-1 worms that have a mild increase in EV release (seen in Chapter 2 and Beer et al., 2018) to allow us to score for an increase or decrease in EV release.

We found that disruption of 17 of the 19 proteins scored did not appear to affect EV release (all 17 had $p>0.05$, Figure 3.1), which suggests that they do not regulate TAT-5 function or EV release. We also found that knockdown of two unnamed proteins,

C44B7.5 and F17E9.4, did cause a significant decrease in EV release with an average of 20±5 and 12±11 EV puncta respectively ($p<0.05$, Figure 3.1), compared to the vector control that had an average of 28±13 EV puncta. This significant decrease in EV release suggests that C44B7.5 and F17E9.4 may function to inhibit TAT-5 and promote EV release.

Initially we did see promising results with an average of 76±93 of EV puncta released when the unnamed protein B0348.2 was knocked down using JA B0348.2 RNAi. However, we were not able to repeat the initial results found JA B0348.2 RNAi and found only an average of 37±23 EV puncta were released. Together these results show that knockdown of B0348.2 by JA RNAi was not found to be significantly different from the vector control (49±58 EV Puncta, $p>0.1$). Further analysis of JA B0348.2 RNAi showed that expressed dsRNA was primarily focused on knocking down the second intron of B0348.2. To create a stronger knockdown, we performed an around the world PCR to create a modified B0348.2 plasmid (LP B0348.2) that primarily targeted B0348.2 exons. We found that LP B0348.2 RNAi treated embryos had an average of 27±14 EV puncta and were not significantly different from vector control treated embryos ($p>0.1$, Figure 3.1). Thus, B0348.2 does not appear to significantly affect TAT-5 function or EV release.

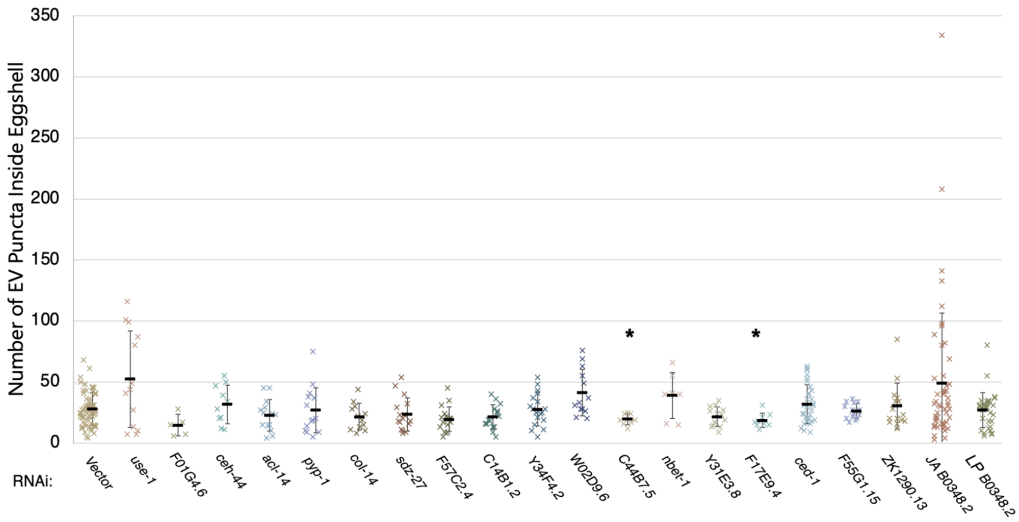

Figure 3.1 Screening EV Release in Transmembrane Proteins with Extracellular Domain

RNAi for listed proteins was performed on GFP::PAD-1 worms. Knockdown of C44B7.5 and F17E9.4 proteins results in a significant decrease in EVs released in treated embryos (*$p<0.05$ compared to empty vector control RNAi). Each data point represents the number of EV puncta in a single embryo. RNAi treated embryos compared to empty vector control using Student's t-test with Bonferroni correction. Mean ± S.D. are shown.

3.3 Discussion

Through the MBMate Y2H, 77 potential TAT-5 interactors were identified. Of those 77 potential interactors, 21 had similar topology to CDC50 family proteins with both transmembrane and extracellular domains. Due to this similarity topology, we hypothesized that these 21 transmembrane proteins with an extracellular domain are more likely to be cofactors/chaperones of TAT-5 compared to other transmembrane without an extracellular domain or other proteins identified in the Y2H screen (Table 3.1).

To test if these proteins have an effect on TAT-5 regulation, we performed an RNAi screen targeting 19 of the 21 transmembrane proteins with an extracellular domain

and scored for their effects on EV release in GFP::PAD-1 mutants. We found that none of the 19 proteins screened cause a significant increase in EV release, which indicates that these proteins are not required for TAT-5 flippase activity. A recent study on TAT-5's yeast ortholog, Neo1, found that isolated Neo1 is still able to bind and flip phospholipids without the presence of PAD-1 or other cofactors (Bai et al., 2021). The same study also did not see a CDC-50 like density in their CryoEM structure (Bai et al., 2021). These results could explain why we are not seeing TAT-5 disruption in our RNAi screen. However, it is still possible for other potential TAT-5 interactors identified in the Y2H screen to be involved in TAT-5 regulation. Therefore, continuing to screen the remaining 61 proteins from the Y2H for changes in EV release may give us more insight into TAT-5 and EV regulation.

Two unnamed proteins, C44B7.5 and F17E9.4, did cause a significant decrease in EV release compared to control. As TAT-5 inhibits EV release, these results suggest that C44B7.5 and F17E9.4 may promote EV release by inhibiting TAT-5. However, it is important to note that the n value for F01G4.6, nbet-1, C44B7.5, and F17E9.4 are fairly low (n=5,7,8 and 9 respectively, Figure 3.1). An important next step for this study is to repeat RNAi for these proteins to further confirm if they have an effect on TAT-5 function or EV release.

Additionally, if C44B7.5 and F17E9.4 or other proteins are found to significantly affect EV release, an interesting approach would be to see if those proteins have any effect on TAT-5 localization. To test this, RNAi can be performed for the proteins of interest on GFP::TAT-5 reporters. It would also be interesting to confirm if *C44B7.5* and

F17E9.4 RNAi are decreased EV release by decreasing PE exposure on the plasma membrane. This can be tested by using duramycin to label and measure externalized PE.

In summary, we have ruled out 19 of the 77 proteins identified by Y2H as cofactors of TAT-5. Further screening and investigation into these proteins and if they are regulating TAT-5 could give us further insight into the mechanisms involved in maintaining lipid asymmetry and EV biogenesis.

Chapter Four: Conserved KLC2-binding and leucine zipper domains of PAD-1 are required to inhibit extracellular vesicle release in *C. elegans* embryos

4.1 Introduction

The Dopey family protein PAD-1 is a key regulator of extracellular vesicle (EV) release in *Caenorhabditis elegans* (Beer et al., 2018; Fazeli et al., 2020). PAD-1 is thought to inhibit EV release by activating the phospholipid flippase TAT-5 to maintain phosphatidylethanolamine (PE) asymmetry in the plasma membrane (Fazeli et al., 2020). When PAD-1 is disrupted, cytofacial PE is externalized, membrane-sculpting ESCRT complexes are recruited to the plasma membrane, and EVs bud from the plasma membrane by ectocytosis (Beer et al., 2018; Beer, 2021).

Dopey family proteins are conserved from yeast to humans and play critical roles in morphogenesis and neural function (Molière et al., 2022). Disruption of Dopey proteins can lead to neurological diseases such as Down syndrome and Peters Anomaly (Rachidi et al., 2009; Darbari et al., 2020) and have been linked to developmental defects during gastrulation (Guipponi et al., 2000). For example, PAD-1 human ortholog, DOPEY2, has increased expression in Down syndrome patients and is found on chromosome 21 (Rachidi et al., 2009). Thus, determining the functions and mechanisms of Dopey family proteins could help our understanding of morphological and neurological diseases. The Dopey protein PAD-1 is a large scaffolding protein with both conserved N- and C-terminal domain (Molière et al., 2022). A partial loss of function is

observed when GFP is knocked into the N-terminus of PAD-1, resulting in a mild increase in EVs and defects in midbody remnant phagocytosis (Fazeli et al., 2020). This suggests that the placement of GFP at the N-terminus of PAD-1 may be disrupting a subset of protein interactions that are required for EV regulation (Beer, 2021; Fazeli et al., 2020). The conserved N-terminus of PAD-1 has a Dopey domain similar to other large Dopey family proteins (Molière et al., 2022), however it is unknown if this domain or other PAD-1 domains are required to inhibit EV release. In mammalian Dopey proteins, the N-terminal Dopey domain binds to the kinesin light chain, KLC2, via a tryptophan surrounded by acidic residues (EWAD motif) (Mahajan et al., 2019; Zhao et al., 2020).

This interaction with KLC2 is proposed to act as a link between the plus-end-directed motor protein Kinesin-1 and membranes for organelle trafficking (Mahajan, et al., 2019; Zhao et al., 2020). However, it is unknown if this interaction or conserved domain is required for EV regulation.

The conserved C-terminal of PAD-1 has a series of leucine zippers that have been shown to play essential roles in Dopey protein function (Molière et al., 2022). A mutation in the leucine zipper domain of Dopey protein DopA (I1695R) disrupts cellular morphogenesis in *Aspergillus nidulans* (Pascon & Miller, 2000). Leucine zippers are typically thought to be involved in protein-protein interactions and dimerization (Landschulz et al., 1988), but it is unknown what proteins interact with this domain.

The goal of this chapter is to determine if the conserved N-terminal EWAD motif or C-terminal leucine zippers of PAD-1 are required to inhibit extracellular vesicle release.

4.2 Results

4.2.1 PAD-1 EWAD Motif is required to inhibit microvesicle release

To determine the role of the KLC2-binding N-terminus in EV release, we used CRISPR/Cas9-mediated genome editing to mutate tryptophan-39 to alanine (W39A) in the EWAD motif of PAD-1(Paix et al., 2014). We found that *pad-1(W39A)* mutants showed sterility and maternal-effect embryonic lethality, similar to previously studied *pad-1* deletion mutants (Beer et al., 2018). To test for an increase in EV release, we crossed the *pad-1(W39A)* mutants with a degron-tagged plasma membrane reporter, mCh::PH::CTPD, allowing us to specifically label EVs released from the plasma membrane. We observed an average of 151±60 EV puncta in *pad-1(W39A)* mutant embryos compared to control embryos with an average of 3±2 EV puncta (Fig. 4.1 A-B, D). EV release in *pad-1(W39A)* mutant embryos is significantly higher compared to control embryos (***$p<0.01$, Figure 4.1). These results demonstrate that the N-terminal EWAD motif is required to inhibit EV release, suggesting that PAD-1 binding to Kinesin-1 could regulate EV release.

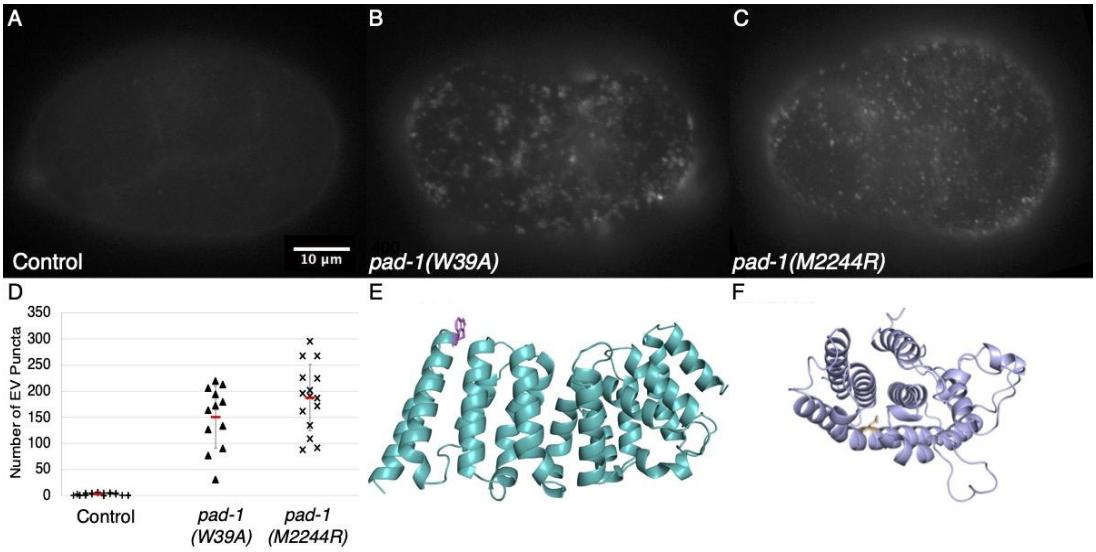

Figure 4.1: Point mutations in PAD-1 KLC2-binding and leucine zipper domains result in a severe increase in EV release.
(A-C) Surface images of of 4-cell embryos expressing mCh::PH::CTPD in control (A), *pad-1(W39A)* KLC2 binding mutant (B), and *pad-1(M2244R)* leucine zipper mutant (C). Scale bar = 10 µm.
(D) The number of mCh::PH::CTPD puncta on top of *pad-1(W39A)* and *pad-1(M2244R)* mutant embryos were significantly increased compared to control embryos (***p<0.001 using one-tailed Student's t-test with Bonferroni correction, control n=22, *pad-1(W39A)* n=12, *pad-1(M2244R)* n=15). EV counts done by Alex Nguyen.
(E) N-terminal Dopey domain (aa16-301 of PAD-1) with W39 highlighted (purple).
(F) C-terminal domain (aa2165-2417 of PAD-1) with M2244 highlighted (beige).
Both images (E and F) are from AlphaFold v2.

4.2.2 PAD-1 C-terminal leucine zippers are required to inhibit EV release

To test a role for the C-terminal leucine zippers in EV release, we again used CRISPR/Cas9-mediated genome editing to mutate methionine-2244 to arginine (M2244R) in the leucine zipper domain of PAD-1(Paix et al., 2014), corresponding to the DopA I1695R mutant previously created by Pascon & Miller, 2000. We discovered that *pad-1(M2244R)* mutants showed sterility and maternal-effect embryonic lethality, similar to *pad-1(W39A)* and deletion mutants (Beer et al., 2018). After crossing the

mCh::PH::CTPD EV reporter with the *pad-1(M2244R)* mutants, we found that the M2244R point mutation resulted in an average of 189±64 EV puncta in embryos compared to control embryos with an average of 3±2 EV puncta (Fig. 4.1 A, C-D). These results show that *pad-1(M2244R)* mutants have a significantly higher increase in EV release compared to control (***$p<0.001$, Figure 4.1) suggesting that the leucine zippers of PAD-1 are crucial for inhibiting EV release by ectocytosis.

4.2.3 Knockdown of Kinesin-1 does not affect EV release

To test the effects of Kinesin-1 on EV regulation, we performed RNAi on both kinesin light chain orthologs, KLC-1 and KLC-2, in a GFP::PAD-1 mutant background. GFP::PAD-1 mutants only have a mild increase in EVs and therefore allowed us to score for an increase or decrease of EVs in RNAi treated embryos compared to vector control. After knocking down Kinesin-1, we found that *klc-1* RNAi had an average of 23±14 EV puncta and *klc-2* RNAi with an average of 35±31 EV puncta (Figure 4.2). These results show that EV release is not significantly different in *klc-1* ($p>0.05$) or *klc-2* ($p>0.1$) RNAi treated embryos compared to vector control that has an average of 28±13 EV puncta (Fig. 4.2). These results suggest that knockdown of *klc-1* and *klc-2* does not affect EV release.

As loss of PAD-1 activity can cause polar body phagocytosis defects, we were curious if Kinesin-1 would also affect phagocytosis. We scored for polar body phagocytosis defects in *klc-1* and *klc-2* RNAi treated embryos and found that *klc-1* and *klc-2* RNAi treated embryos showed embryonic lethality, similar to previous studies

characterizing *klc-1* and *-2* RNAi (Yang et al., 2005), which suggests a successful knockdown of *klc-1* and *klc-2*. We did not see any significant second polar body phagocytosis defects compared to the control in our RNAi treated embryos, as all polar bodies were internalized in *klc-2* RNAi treated embryos (n=41, Figure 4.3) and all but one polar body was internalized in *klc-1* RNAi treated embryos (n=29, Figure 4.3). These results suggest that unlike *pad-1* RNAi (Beer et al., 2018), disruption of *klc-1* and *klc-2* do not disrupt polar body phagocytosis.

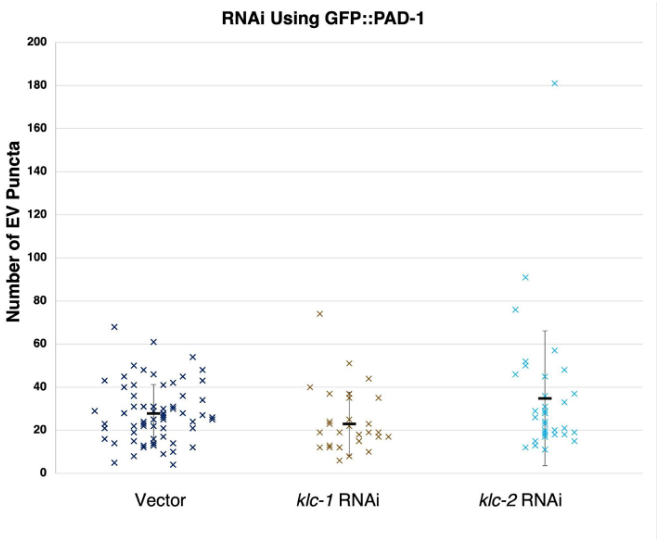

Figure 4.2: Knockdown of Kinesin-1 via KLC-1 or -2 RNAi does not significantly alter EV release.
The number of mCh::PH::CTPD puncta counted in vector control, *klc-1* and *klc-2* RNAi treated embryos was not significantly different from vector control ($p>0.05$, $p>0.1$ using one-tailed Student's t-test with Bonferroni correction). RNAi was performed on GFP::PAD-1 mutant background. Error bars display standard deviation. Each point represents a single embryo.

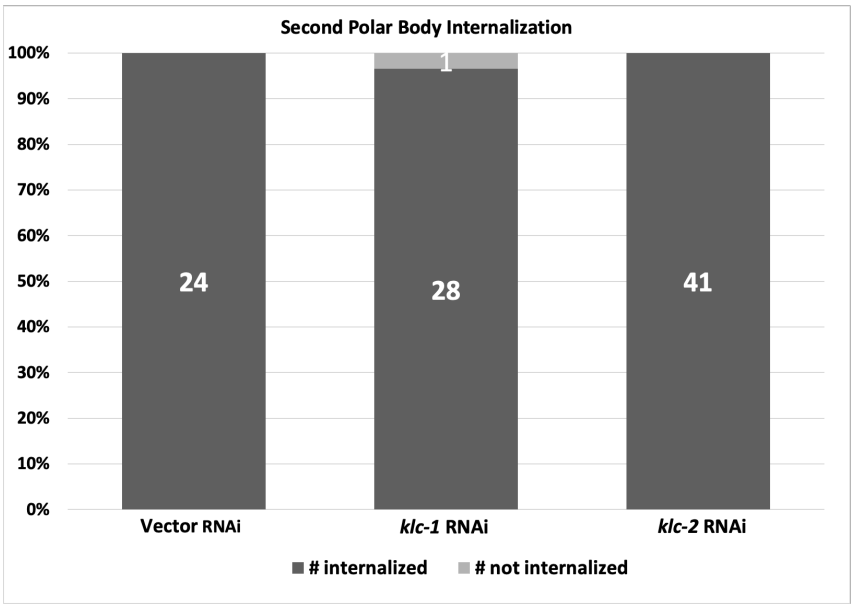

Figure 4.3: klc-1 and klc-2 RNAi does not disrupt polar body Phagocytosis
Second polar bodies tagged with mCh::PH::CTPD reporter were scored for internalization from the late 4- to 15-cell stage. *klc-1* or *klc*-2 RNAi does not disrupt P0 midbody phagocytosis ($p>0.1$). RNAi knockdowns compared to control using Fisher's exact test. Sample size is indicated by the numbers inside the bars.

4.3 Discussion

We found that disrupting both the N- and C-term of PAD-1 by *pad-1(W39A)* and *pad-1(M2244R)* point mutations caused a significant increase in EV release compared to control. These results suggest both the conserved N-term EWAD and C-term leucine zippers of PAD-1 are required to inhibit EV release from the plasma membrane.

We performed *klc-1* and *-2* RNAi using GFP::PAD-1 background to test the effects of Kinesin-1 on EV release and observed that knocking down Kinesin-1 through *klc-1* and *-2* RNAi had no significant effect on EV release. GFP::PAD-1 is known to disrupt phagocytosis of midbody remnants but not polar bodies (Fazeli et al., 2020). We also found that Kinesin-1 RNAi does not affect polar body internalization, which

suggests that PAD-1 is still functioning, as loss of PAD-1 disrupts polar body phagocytosis (Beer et al., 2018).

Two *in vitro* studies on PAD-1 human ortholog DOPEY1 have found that DOPEY1 binds KLC2 through its N-term EWAD motif (Mahajan et al., 2019; Zhao et al., 2020). However, this interaction is debated in PAD-1's other human ortholog DOPEY2, as one study found that DOPEY2 does not bind KLC2 (Mahajan et al., 2019), while the other found that DOPEY2 does bind KLC2 (Zhao et al., 2020). If PAD-1 is ultimately not interacting with Kinesin-1, this could explain why we are not seeing a significant increase in EV release when we knock down Kinesin-1 through *klc-1* and *-2* RNAi. Therefore, it may be of interest to first determine if PAD-1 and Kinesin-1 colocalize in early embryos and then perform a pull-down assay to confirm that they are indeed interacting.

Previous studies have shown that there is redundancy between KLC-1 and -2 (Yang et al., 2005). This redundancy may be why we are not seeing any effects on EV release when we knockdown KLC-1 and -2 alone. In the future a double RNAi to knockdown KLC-1 and -2 can be performed to better understand the functional relationship between KLC-1 and -2 and their effects on EV release and phagocytosis.

Leucine zippers conserved in the C-term of PAD-1 are also shown to play a key role in EV regulation, however it is still unclear what proteins are interacting with this domain. Therefore, it may be of interest to perform a pull-down assay followed by mass spectrometry first with wild type (WT) PAD-1 to see what proteins are associated originally with WT PAD-1, and then again with a *pad-1(M2244R)* mutant. This

experiment could give insight into what PAD-1 leucine zippers region may be interacting with.

Since leucine zippers are thought to be typically involved in protein-protein interaction and dimerization (Landschulz et al., 1988), it is possible that this domain is somehow involved in PAD-1 localization. Therefore to further our understanding PAD-1 an interesting next approach to this study would be to test the effects of PAD-1's leucine zipper domain on PAD-1 localization. This can be done by first characterizing PAD-1's subcellular localization in early embryos, by utilizing strains that have a functional PAD-1 fluorescent knockin like PAD::mScarlet-I and GFP labeled organelle membrane markers. After characterizing where PAD-1 localizes in cells, we could then test the effects of PAD-1's leucine zippers on localization by using CRISPR/Cas9-mediated genome editing to create a fluorescent knockin allele of PAD-1(M2244R).

In conclusion, our study demonstrates that both the conserved N- terminal EWAD and C-terminal leucine zippers of the Dopey protein PAD-1 are required to inhibit EV release from the plasma membrane. However, what proteins are interacting with these domains in PAD-1 has yet to be determined. Further investigation into the protein-protein interactions at these PAD-1 domains could help us further understand the mechanisms that govern EV release and Dopey family protein function.

Chapter Five: Characterizing a gain-of-function allele of PAD-1

5.1 Introduction

Neurons are polarized cells with a highly regulated network of axons and dendrites, collectively known as neurites (Norkett et al., 2020; Stone et al., 2010). Neurites are composed of cytoskeletal components including microtubules, which assist in cargo transport and neurite outgrowth (Norkett et al., 2020; Kapitein and Hoogenraad, 2015; Lu et al., 2013; Winding et al., 2016). Neurite outgrowth is driven by a process known as microtubule sliding, which is the movement of microtubules relative to other microtubules by molecular motors (Norkett et al., 2020). Work in *Drosophila* neurons has identified the highly conserved plus-end-directed motor protein, Kinesin-1, as the molecular motor responsible for powering microtubule sliding, and the kinesin-6 Pavarotti as an molecule responsible for inhibiting microtubule sliding in neurons (Norkett et al., 2020; Del Castillo et al., 2015; Lin et al., 2012; Lu et al., 2013; Winding et al., 2016).

In *C. elegans*, the conserved protein SAX-2 works with the NDR kinase, SAX-1, to maintain and stabilize neuron morphology (Zallen et al., 1999; Zallen et al., 2000; Gallegos et al., 2004). SAX-1 and SAX-2 orthologs have been shown to maintain and stabilize neuron morphology by restricting neurite outgrowth (microtubule sliding) (Norkett et al., 2020; Del Castillo et al., 2015; Lin et al., 2012). SAX-2 orthologs also

regulate the kinase activity of SAX-1 orthologs (Emoto et al., 2004). When SAX-1 or SAX-2 function is lost, neuron morphology is disrupted. For instance, *sax-1* and *sax-2* mutants have been characterized as having expanded cell bodies and ectopic neurites in *C. elegans* (Zallen et al. 1999; Zallen et al., 2000).

SAX-1 and SAX-2 are conserved from yeast to humans (Zallen et al., 2000; Gallegos et al., 2004). In *Drosophila*, SAX-1 and SAX-2 orthologs, Trc and Fry, work together with kinesin-6 Pavarotti (ZEN-4 in *C. elegans*) to inhibit microtubule sliding (Norkett et al., 2020; Del Castillo et al., 2015; Lin et al., 2012). Human and *Drosophila* SAX-1 orthologs, Trc and LATS, have been shown to phosphorylate MKLP1, the human ortholog of Pavarotti and ZEN-4, *in vitro* (Okamoto et al., 2015; Norkett et al., 2020). Knockdown of Pavarotti via RNAi results in axon hyperextension and increased microtubule sliding (Del Castillo et al., 2015; Lin et al., 2012).

Our collaborator, Dr. Seungmee Park in the Chisholm lab at the University of California San Diego discovered a new allele of PAD-1(E1909K) in a screen for suppressors of neuronal morphology defects in *sax-2* mutants. PAD-1(E1909K) is a point mutation of glutamic acid-1909 to lysine outside of the conserved N- and C-term domains of PAD-1. Dr. Park found that when she introduced PAD-1(E1909K) into a *sax-2* mutant background, neurons that normally had expanded cell bodies and ectopic neurites appeared virtually wild type. These findings suggest that PAD-1(E1909K) suppresses the morphological defects caused by loss of SAX-2. As PAD-1 is a key regulator of EV release it is possible that PAD-1(E1909K) may also suppress excess EV

release. However, if PAD-1(E1909K) is a functional PAD-1 allele and how it is rescuing the morphological phenotypes seen in *sax-2* mutants is unknown.

Strong loss of PAD-1 function results in sterility, embryonic lethality, polar body phagocytosis defects, enlarged multivesicular late endosomes, and a severe increased EV release, while partial loss of PAD-1 function only causes a mild increase in EV release and midbody remnants phagocytosis defects (Beer et al., 2018; Fazeli et al., 2020). PAD-1(E1909K) mutants appear to at least have partial PAD-1 function as they are not sterile or embryonic lethal. However, it is unknown if this allele causes any additional PAD-1 loss of function phenotypes.

Thus, the goal of this chapter is to characterize the effects of E1909K mutation on PAD-1 function by examining known PAD-1 loss of function phenotypes.

5.2 Results

5.2.1 PAD-1(E1909K) does not cause a significant increase in EVs

Given that our collaborators observed observed a suppression of neuronal morphology defects when they introduced PAD-1(E1909K) allele is introduced to a *sax-2* mutant background, we speculated that PAD-1(E1909K) allele may have an effect on PAD-1's ability to regulate extracellular vesicle (EV) release. To test this, we crossed *pad-1(E1909K)* mutants with a degron-tagged plasma membrane reporter, mCh::PH::CTPD, to allow us to visualize and label EVs released from the plasma membrane (Beer et al., 2019). We found that *pad-1(E1909K)* mutants had an average of 1±1 EV puncta and control embryos had an average of 1±2 EV puncta (Figure 5.1 A-B,

and E). Thus, *pad-1(E1909K)* mutants are not significantly different from the control ($p>0.5$, Figure 5.1 A-B, and E), suggesting that PAD-1(E1909K) does not disrupt PAD-1 function in EV regulation.

5.2.2 PAD-1(E1909K) causes a significant decrease in EVs released in GFP::PAD-1 embryos

As wild type embryos only release a few EVs, it is difficult to score for a significant loss in EVs. Therefore, we were curious to see if this new PAD-1 allele would have any effect on EV release in a PAD-1 partial loss of function background. To test this Dr. Park created GFP::PAD-1(E1909K) using CRISPR/Cas9-mediated genome editing (Paix et al., 2014). After crossing GFP::PAD-1(E1909K) mutants with mCh::PH::CTPD degron tag, we found that GFP::PAD-1(E1909K) embryos had a significant decrease in EV puncta (3±2, $p<0.01$) compared to GFP::PAD-1 control embryos (20±16, Figure 5.1 C-E). These findings further suggest that PAD-1(E1909K) increases PAD-1's ability to inhibit EV release and suggests that PAD-1(E1909K) is a gain of function allele.

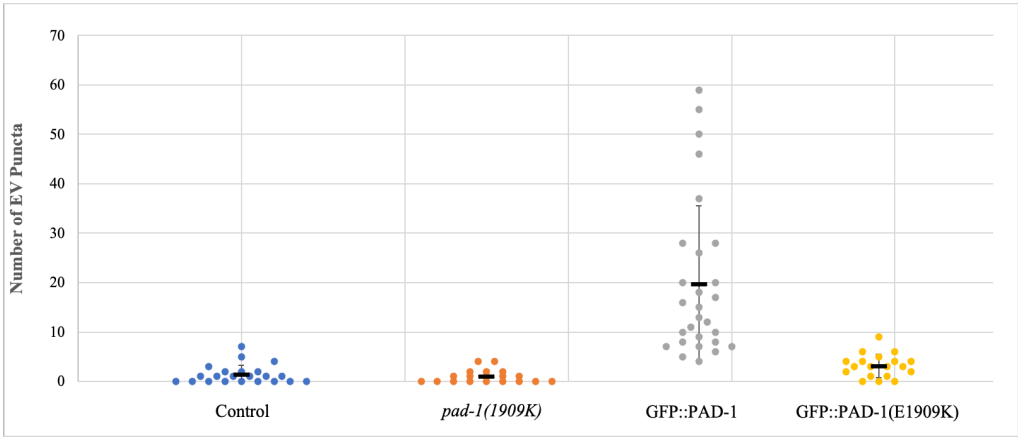

Figure 5.1 PAD-1(E1909K) significantly decrease EV released
(A-C) Images of 4-cell embryos expressing mCh::PH::CTPD in control (A), *pad-1(E1909K)* (B), GFP::PAD-1 (C), and GFP::PAD-1(E1909K) (D). Scale bar = 10 µm. D) The number of mCh::PH::CTPD EV puncta inside the eggshell of *pad-1(E1909K)* mutant embryos is not significantly different from control embryos ($p>0.05$). GFP::PAD-1(E1909K) embryos have significantly less mCh::PH::CTPD EV puncta compared to GFP::PAD-1 embryos. Each data point represents the number of EV puncta observed in one embryo. Mutants compared using Student's t-test with Bonferroni correction. Mean ± S.D. are shown with the black vertical bars.

5.2.3 Knockdown of sax-2 does not significantly affect EV release

As PAD-1(E1909K) is suppressing morphological effects in sax-2 mutants, we hypothesize disruption of *sax-2* may cause an increase in EV release. To test SAX-2 effects on EV release, we performed *sax-2* RNAi on a GFP::PAD-1 mutant background. RNAi was performed on GFP::PAD-1 mutants because these mutants have been shown to have a mild increase in EV release (Seen in Chapter 2 and Fazeli et al., 2020), which allowed us to score for an increase or decrease in RNAi treated embryos compared to vector control. After knocking down *sax-2* we found that *sax-2* RNAi embryos had an average of 25±12 EV puncta (Figure 5.2) and vector control RNAi embryos had an average of 27±13 EV puncta (Figure 5.2). These results demonstrate that *sax-2* RNAi

does not cause a significant difference in EV release compared to vector control ($p>0.1$), Figure 5.2) and suggests that SAX-2 does not regulate EV release.

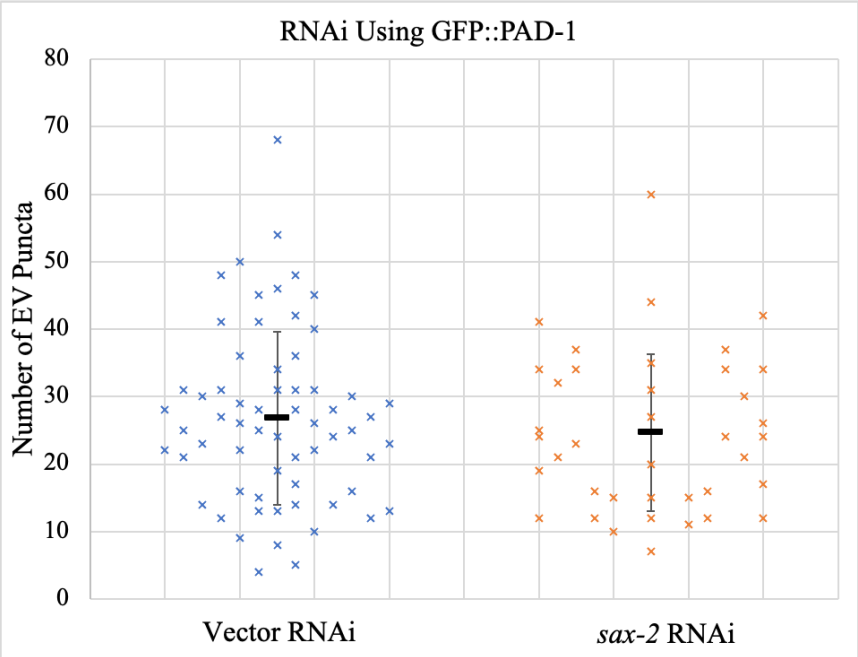

Figure 5.2 Knockdown of sax-2 via RNAi does not affect EV release
RNAi was used to knockdown *sax-2* in GFP::PAD-1 mutants.The number of mCh::PH::CTPD puncta counted in *sax-2* RNAi treated embryos was not significantly different from vector control ($p>0.05$). Each point represents a single embryo. Mean ± S.D. are shown

5.2.4 PAD-1(E1909K) does not disrupt phagocytosis of polar bodies

Having established that *pad-1(E1909K)* mutants do not have an increase in EV release, we next wanted to look at other severe loss of PAD-1 function PAD-1 phenotypes, such as disrupted polar body phagocytosis. To do this, we scored second polar body labeled with mCh::PH::CTPD for internalization in *pad-1(E1909K)* mutant embryos. We found that all polar bodies were internalized in *pad-1(E1909K)* mutant

(n=19, Figure 5.3). This data suggests that *pad-1(E1909K)* does not disrupt cell corpse phagocytosis.

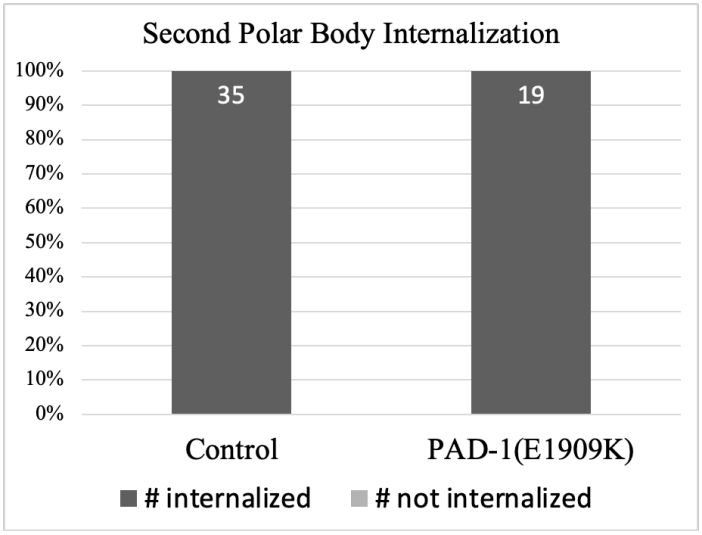

Figure 5.3: PAD-1(E1909K) does not affect second polar body internalization
Polar bodies labeled with mCh::PH::CTPD were scored for internalization from the late 3- to 15-cell stage. PAD-1(E1909K) does not disrupt second polar body phagocytosis ($p>0.1$). Mutant compared to control using a Fisher's exact test.

5.2.5 PAD-1(E1909K) does not disrupt phagocytosis of P0 midbody remnants

We were also curious to see if *pad-1(E1909K)* mutants had partial loss of PAD-1 function phenotype, such as defects in midbody remnant phagocytosis. We used mCherry fluorescently tagged NMY-2 (non-muscle myosin) to label P0 midbody remnants released during embryonic division in *C. elegans* embryos (Shelton et al., 1999; Fazeli et al., 2020). A P0 midbody remnant is the first embryonic midbody released during division of zygote P0 into the AB (anterior blastomere) and P1 (posterior blastomere), and is phagocytosed by one of the daughter cells (Green et al., 2013; Ou et al., 2014;

Fazeli et al., 2016). We found that *pad-1(E1909K)* mutants had no defects in midbody phagocytosis, as all P0 midbody remnants were engulfed (n=16, Figure 5.4 A-C).

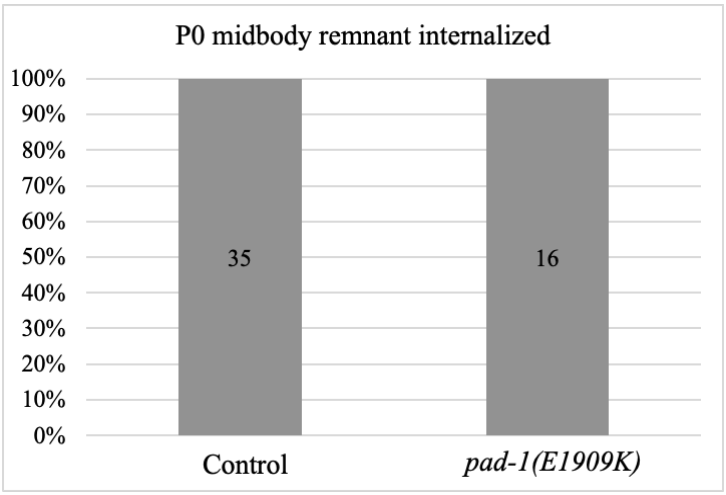

Figure 5.4 PAD-1(E1909K) does not affect P0 midbody phagocytosis
(A-B) P0 midbody remnants labeled with NMY-2::mCherry in 4-cell control (A) and PAD-1(E1909K) embryos (B).
C) P0 midbody remnants tagged with NMY-2::mCherry reporter were scored for internalization from the late 4- to 24-cell stage. PAD-1(E1909K) does not disrupt P0 midbody phagocytosis ($p>0.1$). Mutant compared to control using a Fisher's exact test. Sample size is indicated by the numbers inside the bars.

5.2.6 PAD-1(E1909K) does not disrupt late endosome size in early *C. elegans* embryos

We next investigated if PAD-1(E1909K) had any effect on multivesicular bodies (MVBs) morphology. Previous studies have found that knockdown of *pad-1* via RNAi results in significantly enlarged LMP-1+ MVBs that appear to group together at cell contacts (Beer et al., 2018). We used GFP fluorescently tagged LMP-1 to label late endosomes or lysosomes. We observed that MVBs in *pad-1(E1909K)* mutant embryos appeared to be similarly sized and located to control (n=10, Figure 5.5 D-E) This data

suggesting that PAD-1(E1909K) does not affect LMP-1 positive late endosomes or lysosomes size. Thus, PAD-1(E1909K) appears to be a functional PAD-1 allele.

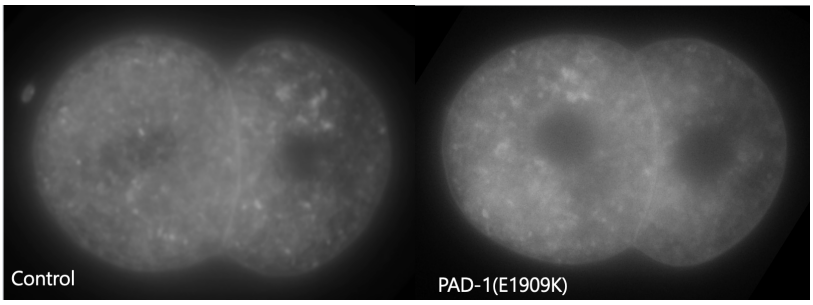

Figure 5.5 PAD-1(E1909K) does not disrupt MVB size
A-B) LMP-1-positive late endosomes or lysosomes labeled with LMP-1::GFP in 2-cell control embryo (A) and *pad-1(E1909K)* embryos (B). LMP-1-positive vesicles are not enlarged in pad-1(E1909K) mutant embryos. (n=10)

5.3 Discussion

Our collaborators observed that PAD-1(E1909K) rescued morphological defects in *sax-2* mutants, however if PAD-1(E1909K) disrupted PAD-1 function was unknown. To confirm that PAD-1(E1909K) is a functional allele we tested for PAD-1 severe and partial loss of function phenotypes (Beer et al., 2018; Fazeli et al., 2020). We found that PAD-1(E1909K) mutants do not have any characterized severe or partial loss of function phenotypes, including increased EV release, phagocytosis defects, or enlarged multivesicular late endosomes. PAD-1(E1909K) worms are also not sterile or embryonic lethal. Therefore PAD-1(E1909K) does not disrupt PAD-1 and is a functional PAD-1 allele.

Crossing PAD-1(E1909K) into GFP::PAD-1 mutants resulted in a significant decrease in EV release. This data shows that PAD-1(E1909K) further inhibited EV release in GFP::PAD-1 mutants and suggests that PAD-1(E1909K) is a gain of function allele. However, how PAD-1(E1909K) is rescuing the effects seen in *sax-2* mutants is still unknown.

PAD-1 has been shown to regulate phosphatidylethanolamine (PE) asymmetry in the plasma membrane by activating TAT-5 (Beer et al., 2018). An interesting next approach to this study would be to test the effects of PAD-1(E1909K) on PE externalization. This can be done by using duramycin to stain PE externalized on the outer leaflet of the plasma membrane (Stafford and Thorpe, 2011). As TAT-5 and PAD-1 regulate EV release by inhibiting PE exposure we propose that PAD-1(E1909K) will decrease PE exposed on the outer leaflet of the plasma membrane.

We also tested the effects of SAX-2 on EV biogenesis by knocking down *sax-2* via RNAi. We found that sax-2 RNAi does not significantly alter EV release in GFP::PAD-1 mutants compared to control. Since RNAi experiments are only a partial knockdown of sax-2, it may be of interest to test EV release in SAX-2 null mutants by crossing mutants with an EV degron reporter.

In conclusion, PAD-1(E1909K) does not exhibit any known PAD-1 loss of function phenotypes but does appear to cause a significant decrease in EVs released in GFP::PAD-1 mutants, suggesting PAD-1(E1909K) is a gain of function allele. However, how PAD-1(E1909K) is rescuing neuronal morphology and decreasing EV release is

unknown. Therefore, furthering our understanding of how PAD-1(E1909K) is functioning could help us understand PAD-1's role and EV biogenesis.

Chapter 6: Conclusions

Extracellular vesicles are released by cells and are involved in many physiological processes including communication and development. Our goal was to further characterize TAT-5 and PAD-1 in order to better understand how they regulate EV release *in vivo*. To do this, we first characterized different TAT-5 point mutations. In chapter 2 we found TAT-5 predicted ATP-binding (F570A) point mutation and predicted PI4P-binding (K1059R) point mutations are fertile and do not disrupt phagocytosis or EV release but do have reduced progeny. TAT-5(D244T), on the other hand, was found to cause embryonic lethality and disrupted both phagocytosis and EV release. Together these data suggest that TAT-5(F570A), TAT-5(K1059R), and TAT-5(D244T) are partial loss of function alleles affecting TAT-5 function to differing extents.

We also characterized TAT-5 and PAD-1 fluorescent knock-ins GFP::TAT-5, PAD-1::mScarlet, and PAD-1::mScarlet-I in chapter 2. We found that these tags do not disrupt TAT-5 or PAD-1 function, unlike GFP::PAD-1, and therefore can be used to further study TAT-5 and PAD-1 localization and protein interactions.

As other P4-ATPases have been shown to require a cofactor for proper localization and flippase activity, we hypothesized that TAT-5 may have a cofactor as well. In chapter 3, we screened for potential cofactors of TAT-5 using RNAi we identified 2 potential TAT-5 inhibitors. However, further experimentation is necessary to confirm these results. Recent studies have shown that the TAT-5 yeast ortholog, Neo1,

does not require a β-subunit to bind and flip PE (Bai et al., 2021). Therefore, TAT-5 may not require a cofactor to recognize and flip PE.

PAD-1 is a known activator of the lipid flippase TAT-5 and inhibits the release of extracellular vesicles via ectocytosis (Beer et al., 2018; Beer, 2021). However, the mechanism by which PAD-1 regulates TAT-5 or EV release is unknown. In chapter 4, we identified key residues important for PAD-1's ability to regulate EV release by TAT-5. By creating point mutations in PAD-1's conserved N- and C-terminal domains, we discovered that PAD-1 conserved N-term EWAD motif and C-term leucine zippers are required to inhibit EV release from the plasma membrane.

Lastly, in chapter 5 we characterized a point mutation outside of the conserved N- and C-term domains of PAD-1, PAD-1(E1909K). Dr. Seungmee Park in the Chisholm lab at the University of California San Diego discovered PAD-1(E1909K) and found that this allele suppressed neurological defects seen in *sax-2* mutants. By scoring for known PAD-1 loss-of-function phenotypes, we determined that PAD-1(E1909K) is not a loss-of-function allele. We did find PAD-1(E1909K) is a gain-of-function allele that can successfully decrease EV release. Further understanding into the mechanisms of how this allele is functioning could broaden our understanding of PAD-1 function in EV biogenesis.

With this work we have successfully identified 3 key domains of PAD-1 required for EV regulation and characterized alleles that can be used to further test TAT-5 and PAD-1 roles in EV biogenesis. As TAT-5 and PAD-1 are conserved in animals, our study not only broadens our understanding of EV biogenesis in *C. elegans* but is likely to be relevant in humans as well.

Chapter Seven: Methods

7.1 Worm culture and strains

C. elegans strains were maintained on Nematode Growth Media (NGM) seeded with OP50 bacteria at room temperature using standard protocols (Brenner 1974). Strains used in this study are listed in Table 7.1

Sterile and embryonic lethal mutants were maintained as heterozygotes by crossing with a genetic balancer strain. Genetic balancers are chromosomal rearrangements that allow lethal or sterile mutations to be stably maintained in heterozygotes by suppressing meiotic recombination (Ahringer 2006). In this study, we used the chromosomal rearrangements tmC18 or tmC27 and translocation rearrangements hT2. The balancers tmC18[dpy-5(tmIs1200[myo-2p::Venus])] and tmC27[unc-75(tmIs1239[myo-2p::Venus]) have a chromosomal rearrangement chromosome I and were used to maintain sterile and lethal mutants on chromosome I (Dejima et al., 2018). The balancer hT2[bli-4(e937) let-?(q782) qIs48] has a chromosome translocation at both chromosome I and III and was used to maintain mutants on chromosome I and III (Edgley et al., 2006).

Table 7.1: Worm strains used in this study.

Strain	Genotype	Source
N2	*Wild Type*	Brenner, 1974
CZ28652	*pad-1(ju1806[E1909K]) zdIs5[mec-4p::GFP + lin-15(+)] I*	Andrew Chisholm
CZ28654	*pad-1(gk125921[E1909K]) I*	Andrew Chisholm
FT166	*unc-119(ed3) III; xnIs65[nmy-2-gfp-zf1, unc-119(+)] IV*	Fazeli et al., 2016
FT207	*tat-5(tm1741) I / hT2[bli-4(e937) let-?(q782) qIs48] (I; III)*	Wehman et al., 2011
FT23	*unc-119(ed3) xnIs8[pJN343: nmy-2::NMY-2-mCherry; unc-119(+) line 26B] III*	Nelson et al., 2011
FX30208	*tmC27[unc-75(tmIs1239[myo-2p::Venus])] I*	Dejima K, et al., 2018
LP162	*nmy-2(cp13[nmy-2::gfp::3XFLAG + LoxP]) I*	Dickinson et al., 2013
MCP6	*pad-1(babIs1[GFP]) I*	Beer et al., 2018
PHX1681	*pad-1(syb1647[M2244R])/+ I*	SunyBiotech
PHX2032	*pad-1(syb2032[W39A])/+ I*	SunyBiotech
PHX2406	*tat-5(syb2406[F570A]) I*	SunyBiotech
PHX2414	*tat-5(syb2414[D244T]) I*	SunyBiotech
PHX2519	*tat-5(syb2519[E246Q])/tmC18[dpy-5(tmIs1200[myo-2p::Venus])] I*	SunyBiotech
PHX2596	*tat-5(syb2414[D244T])/tmC18[dpy-5(tmIs1200[myo-2p::Venus])] I*	SunyBiotech
PHX2617	*tat-5(syb2617[K1059R]) I*	SunyBiotech
PHX2620	*tat-5(syb2617[K1059R]) / tmC18[dpy-5(tmIs1200[myo-2p::Venus])] I*	SunyBiotech
PHX2858	*pad-1(syb2858[pad-1::wrmScarlet]) I*	SunyBiotech

PHX4112	*pad-1(syb4112[pad-1::attB1::GLO-mScarlet-I]) I*	SunyBiotech
WEH350	*wurIs118[lmp-1::TY1::GFP::FLAG fosmid, unc-119(+)] I; unc-119(ed3) III*	Fazeli et al., 2022
WEH430	*unc-119(ed3) xnIs8[pJN343: nmy-2::NMY-2::mCherry; unc-119(+)] III; xnIs65[nmy-2::gfp::zf1, unc-119(+)] IV*	Beer et al., 2019
WEH434	*unc-119(ed3) III; wurIs155[pAZ132-coPH-oma-1(219-378): pie-1::mCh::coPH::CTPD; unc-119(+)]*	Beer et al., 2019
WEH490	*pad-1(syb1647[M2244R]) / hT2[bli-4(e937) let-?(q782) qIs48] I; + / hT2 III*	Crossed N2 to FT207, then PHX1681
WEH493	*pad-1(syb1647[M2244R]) / tmC27[unc-75(tmIs1239[myo-2p::Venus])] I*	Crossed N2 to WEH490, then FX30208
WEH516	*pad-1(syb2032[W39A]) / tmC27[unc-75(tmIs1239[myo-2p::Venus])] I*	Crossed N2 to FX30208, then PHX2032
WEH578	*tat-5(wur36[GFP::tat-5 + loxP]) I; unc-119(ed3) III*	Injection
WEH584	*tat-5(wur36[GFP::tat-5 + loxP]) I*	Outcrossed WEH578 2x to N2
WEH591	*tat-5(wur36[GFP::tat-5 + loxP]) I; unc-119(ed3) III; wurIs155[pAZ132-coPH-oma-1(219-378): pie-1::mCh::coPH::CTPD; unc-119(+)]*	Crossed WEH584 x WEH434
WEH592	*tat-5(wur36[GFP::tat-5 + loxP]) I; wurIs158[pAZ132-coPH-oma-1(219-378): pie-1::mCh::coPH::CTPD; unc-119(+)]*	Crossed WEH585 x WEH438
WEH593	*tat-5(wur36[GFP::tat-5 + loxP]) I; unc-119(ed3) xnIs8[pJN343: nmy-2::NMY-2::mCherry; unc-119(+)] III*	Crossed N2 x WEH430 x WEH584
WEH594	*tat-5(syb2414[D244T])/tmC18[dpy-5(tmIs1200[myo-2p::Venus])] I; xnIs65[nmy-2::gfp::zf1, unc-119(+)] IV*	Crossed N2 x WEH430 x PHX2596

WEH595	*tat-5(syb2414[D244T])/tmC18[dpy-5(tmIs1200[myo-2p::Venus])] I; unc-119(ed3) xnIs8[pJN343: nmy-2::NMY-2::mCherry; unc-119(+)] III*	Crossed N2 x WEH430 x PHX2596
WEH599	*tat-5(syb2414[D244T])/tmC18[dpy-5(tmIs1200[myo-2p::Venus])] I; wurIs155[pAZ132-coPH-oma-1(219-378): pie-1::mCh::coPH::CTPD; unc-119(+)]*	Crossed WEH434 x PHX2596
WEH619	*pad-1(syb2858[pad-1::wrmScarlet]) I; unc-119(ed3) III; wurIs155[pAZ132-coPH-oma-1(219-378): pie-1::mCh::coPH::CTPD; unc-119(+)]*	Crossed N2 x PHX2858, then WEH434
WEH620	*tat-5(syb2617[K1059R]) I; unc-119(ed3) III; wurIs155[pAZ132-coPH-oma-1(219-378): pie-1::mCh::coPH::CTPD; unc-119(+)]*	Crossed N2 x PHX2617, then WEH434
WEH621	*nmy-2(cp13[nmy-2::gfp::3XFLAG + LoxP]) pad-1(syb2858[pad-1::wrmScarlet]) I*	Crossed N2 x PHX2858, then LP162
WEH623	*pad-1(syb2858[pad-1::wrmScarlet]) I*	Outcrossed 4X to N2
WEH624	*tat-5(syb2406[F570A]) I; unc-119(ed3) III; wurIs155[pAZ132-coPH-oma-1(219-378): pie-1::mCh::coPH::CTPD; unc-119(+)]*	Crossed N2 x PHX2406, then WEH434
WEH642	*pad-1(babIs1[GFP]) I; unc-119(ed3)? III; wurIs155[pAZ132-coPH-oma-1(219-378): pie-1::mCh::coPH::CTPD; unc-119(+)]*	Crossed MCP6 males x WEH434.
WEH652	*nmy-2(cp13[nmy-2::gfp::3XFLAG + LoxP]) pad-1(syb4112[pad-1::attB1::GLO-mScarlet-I]) I*	Crossed PHX4112 x N2 2X, then LP162
WEH653	*pad-1(syb4112[pad-1::attB1::GLO-mScarlet-I]) I; unc-119(ed3)? III; wurIs155[pAZ132-coPH-oma-1(219-378): pie-1::mCh::coPH::CTPD; unc-119(+)]*	Crossed PHX4112 x N2 2X, then WEH434
WEH659	*pad-1(syb1647[M2244R]) / tmC27[unc-75(tmIs1239[myo-2p::Venus])] I; unc-119(ed3) III; wurIs155[pAZ132-coPH-oma-1(219-378): pie-1::mCh::coPH::CTPD; unc-119(+)]*	Crossed N2 to WEH493, then WEH434

WEH660	*pad-1(syb2032[W39A]) / tmC27[unc-75(tmIs1239[myo-2p::Venus])] I; unc-119(ed3)? III; wurIs155[pAZ132-coPH-oma-1(219-378): pie-1::mCh::coPH::CTPD; unc-119(+)]*	Crossed N2 to WEH516, then WEH434
WEH667	*pad-1(gk125921[E1909K]) I; unc-119(ed3)? III; wurIs155[pAZ132-coPH-oma-1(219-378): pie-1::mCh::coPH::CTPD; unc-119(+)]*	Crossed WEH434 x CZ28654.
WEH668	*pad-1(ju1806[E1909K]) zdIs5[mec-4p::GFP + lin-15(+)] I; unc-119(ed3)? III; wurIs155[pAZ132-coPH-oma-1(219-378): pie-1::mCh::coPH::CTPD; unc-119(+)]*	Crossed WEH434 x CZ28652.
WEH670	*pad-1(ju1806[E1909K]) zdIs5[mec-4p::GFP + lin-15(+)] wurIs118[lmp-1::TY1::GFP::FLAG fosmid, unc-119(+)] I*	Crossed CZ28652 x WEH350.
WEH671	*pad-1(ju1806[E1909K]) zdIs5[mec-4p::GFP + lin-15(+)] I; unc-119(ed3) xnIs8[pJN343: nmy-2::NMY-2::mCherry; unc-119(+)] III*	Crossed CZ28652 x WEH430
WEH680	*pad-1(babIs1[GFP] ju1881[E1909K]) I; unc-119(ed3)? III; wurIs155[pAZ132-coPH-oma-1(219-378): pie-1::mCh::coPH::CTPD; unc-119(+)]*	Cross CZ28928 x WEH434

7.2 Crossing worm strains

To cross worm strains, L4 hermaphrodites were heat shocked at 33°C for 4 hours to create male progeny. Male progeny were then picked 3 days after heat shock. To produce more male offspring, male worms isolated from heat shock plate were picked onto a cross plate and allowed to mate with L4 hermaphrodites of the same strain. A higher frequency of males is produced between male and hermaphrodite reproduction as male-derived sperm outcompetes hermaphrodite-derived sperm during fertilization (Ward

& Carrel, 1979). After 3 days, L4 male progeny were picked onto a cross plate with 4 L4 hermaphrodites of the other stain. After allowing to mate for 2 days, F0-generation hermaphrodites were separated into individual plates and F1-generation progeny were screened for males to identify a successful mating. Once a successful mating was identified, F1-generation hermaphrodites at L4 larval stage were isolated from male siblings to avoid re-mating and allowed to self-fertilize. Homozygous worms were identified by genotyping F1-F3-generation hermaphrodite progeny or by scoring fluorescence using a Zeiss Axio Observer 7 inverted microscope.

7.3 Genotyping worms by PCR

Adult hermaphrodite worms were lysed in 5µl single worm lysis buffer. After lysing, worm DNA was amplified by polymerase chain reaction (PCR). DNA polymerase used in this study to perform PCR was 2X OneTaq polymerase (New England BioLabs). All conditions including annealing temperatures and extension times for each experiment was based on primers and size of region of interest. Primers used in this study are listed in Table 7.2

Restriction enzymes were used to identify transgenes in genotyping of TAT-5(D2244T), PAD-1(M2244R), PAD-1(E1909K), and TAT-5(K1059R). The *tat-5(D2244T)* mutation was digested with AgeI (New England BioLabs) at 37°C for 15 minutes. The *pad-1(E1909K)* mutation was digested with HinfI (New England BioLabs) at 54°C for 1 hour and 15 minutes. The *pad-1(M2244R)* mutation was digested with BstEII (New England BioLabs) at 37°C for 1 hour. The *pad-1(W39A)* mutation was

digested with BstEII (New England BioLabs) at 37°C for 1 hour. The *tat-5(K1059R)* mutation was digested with HaeIII (New England BioLabs) at 37°C for 1 hour and 5 minutes.

Table 7.2: Primers used to genotype worm strains.

Primers	Sequence	Genotyped Allele
pad-1 3'UTR R2	TCCA CAA TTT CCA CGA GAT ATG TAC	syb2858
GLO-mSc-N R	CAGCTTGGCGGTCTGAGTT	syb2858
GLO-mSc-C F	GGCGGATTTCAAGACCACAT	syb2858
pad-1 downstream R	TCG CCA TTT TCT TGC CAG TTG T	syb4112
attB1	ggggacaagtttgtacaaaaaagcaggct	syb4112
tat-5 TM10 F	ggccatcacagcagtctcat	syb2617
tat-5 3'UTR R3	gttgcgagtgggggaagaat	syb2617
tat-5 F570 RFLP R	CCC ATT CGT TTT GTT TCT GAT GTA	syb2406
tat-5 exon 6 F3	GGC ACT CGT TCT CTG CTA A	syb2406
pad-1 exon 23 F	ctccggaagccttacctacaa	syb2858
wrmScarlet N R	GTTTGGGTTCCCTCGTATGGA	syb2858
wrmScarlet C F	GTTACCTCGCCGACTTCAAGA	syb2858
tat-5 exon 5 R KpnI	CCG GTA CCT TTC ATG GCA ACC ATA ACC	syb2414
tat-5 geno F	TGC TCC AAT CAC TTA CTG GGG AC	syb2414
pad-1 promoter F4	CCG TAA CAT TTC TCA ACT TTC TGC T	syb2032
pad-1 exon 2 R	GCT GGA TGA AGG CAT TGT GAC A	syb2032
pad-1 syb1647 F	GGGTCTCACGGCGAAAATA	syb1647
syb1647 BstEII R	CGTGAACGAGCTCGGTAAC	syb1647

attB1 pad-1 DEC F4	GGGGACAACTTTGTACAAAAAAGTTGtct catattctccgaacacctcctt	syb2521
pad-1 M2244R R	CACCAATCAAACTGTGTG	syb2521
pad-1 exon 18 HinfI R	CGACAATTGCATTGACGGATT	gk125921 or ju1806
oSP186 F	cagaatcctgagtgactttgtga	gk125921 or ju1806

7.4 CRISPR/Cas9-mediated genome editing

TAT-5 and PAD-1 point mutation mutants and fluorescent knock-in mutants were created by Sunybiotech using CRSIPR-Cas9 methodology (Paix et al. 2014). The PAD-1 KLC binding mutant W39A (PHX2032 pad-1(syb2032[W39A])/+ I) was generated by CRISPR using Sg1: ATTCGAAACACCCAATGAATGGG. The oligo TGCTGGATGAAGGCATTGTG was used as a repair template.

The PAD-1 leucine zipper domain mutant M2244R (PHX1681 pad-1(syb1647)/+) was generated by CRISPR using Sg1: GATTGGTGTGTGGCCTATTATGG. The repair template used was GTACTTCTTCTCCGACTCCGCCCACACAGTTTGATTGGTGTGTGGCCTATACG CGTTACAGAGCTCGTTCACGCACTATCACAGCTTGAACAACAATTACAAAG.

The TAT-5 Phenylalanine mutant in ATP-binding region F570A (PHX2406 tat-5(syb2406[F570A]) I) was generated by CRISPR. Synonymous mutations are labeled in blue.

syb2406:

TGTTCAACTT**CCT**AATGGACAGACATTGATGAAACAATTCCAGATTCTTTATG

TATTC**CCGGCT**ACATCAGAAACAAAACGAATGGGAATTATTGTGAAAGACG

AGACAACTGATGAAGTTACACTTTTAATGAAAGGAGCTGATACTGTAATGAG

TGGAATGGTTCAATATAATGATTGGTTAGATGAA**GAG**TGTAGTAATA

Wild Type:

TGTTCAACTT**CCA**AATGGACAGACATTGATGAAACAATTCCAGATTCTTTATG

TATTC**CCATTT**ACATCAGAAACAAAACGAATGGGAATTATTGTGAAAGACGA

GACAACTGATGAAGTTACACTTTTAATGAAAGGAGCTGATACTGTAATGAGT

GGAATGGTTCAATATAATGATTGGTTAGATGAA**GAA**TGTAGTAATA

The TAT-5 predicted PI4P-binding mutant K1059R (PHX2620 tat-5(syb2617[K1059R]) / tmC18[dpy-5(tmIs1200[myo-2p::Venus])] I) was generated by CRISPR. Synonymous mutation is labeled in blue.

syb2617: ATTATACATT**GTCAGA**GCCCTACGAC

Wild Type: ATTATACATT**GTAAAG**GCCCTACGAC

The PAD-1 c-terminal wrmScarlet mutant PAD-1::wrmScarlet (PHX2858 pad-1(syb2858[pad-1::wrmScarlet]) I) was generated by CRISPR. Synonymous mutation is labeled in blue.

syb2858:

CCGACTCGAA**TCT**GCTCTCTACGTGGATTTTTCTGAACATTTGCAATTTCTTG

GAGGAGGAGGATCTGGAGGAGGAGGATCTGGAGGAGGAGGATCTGCTGCTG

CTATGGTCAGCAAGGGAGAGGCAGTTATCAAGGAGTTCATGCGTTTCAAGGT

CCACATGGAGGGATCCATGAACGGACACGAGTTCGAGATCGAGGGAGAGGG

AGAGGGACGTCCATACGAGGGAACCCAAACCGCCAAGCTCAAGGTCACCAA

GGGAGGACCACTCCCATTCTCCTGGGACATCCTCTCCCCACAATTCATGTACG

GATCCCGTGCCTTCACCAAGCACCCAGCCGACATCCCAGACTACTACAAGCA

ATCCTTCCCAGAGGGATTCAAGTGGGAGCGTGTCATGAACTTCGAGGACGGA

GGAGCCGTCACCGTCACCCAAGACACCTCCCTCGAGGACGGAACCCTCATCT

ACAAGGTCAAGCTCCGTGGAACCAACTTCCCACCAGACGGACCAGTCATGCA

AAAGAAGACCATGGGATGGGAGGCCTCCACCGAGCGTCTCTACCCAGAGGA

CGGAGTCCTCAAGGGAGACATCAAGATGGCCCTCCGTCTCAAGGACGGAGG

ACGTTACCTCGCCGACTTCAAGACCACCTACAAGGCCAAGAAGCCAGTCCAA

ATGCCAGGAGCCTACAACGTCGACCGTAAGCTCGACATCACCTCCCACAACG

AGGACTACACCGTCGTCGAGCAATACGAGCGTTCCGAGGGACGTCACTCCAC

CGGAGGAATGGACGAGCTCTACAAGTAAaagtgtctgt

The PAD-1 c-terminal mScarlet-I mutant PAD-1::mScarlet-I (PHX4112 pad-1(syb4112[pad-1::attB1::GLO-mScarlet-I]) was generated by CRISPR. Synonymous mutation is labeled in blue.

syb4112:

CCGACTCGAA**TC**TGCTCTCTACGTGGATTTTTCTGAACATTTGCAATTTCAAT

GCTTTTTTATAATGCCAACTTTGTACAAAAAAGCAGGCTGCTCTTCGATGGTC

TCCAAAGGAGAAGCTGTGATCAAGGAGTTCATGCGCTTCAAGGTTCACATGG

AAGGAAGCATGAATGGTCACGAGTTCGAAATCGAAGGAGAAGGGGAGGGCC

GCCCGTACGAGGGAACTCAGACCGCCAAGCTGAAGGTCACCAAGGGAGgtaagt

ttgtgataatccaatttcaattcgcaatggtcatcgttttttcagGACCACTTCCATTCTCATGGGATATTCT

CTCCCCACAATTCATGTACGGCTCCCGTGCTTTCATCAAACACCCAGCCGACA

TTCCAGATTACTACAAGCAATCTTTCCCAGAAGGCTTCAAGTGGGAGCGTGT

GATGAACTTCGAGGATGGTGGAGCAGTTACAGTAACTCAGGACACTTCTCTC

GAGgtaagtttttactccgcttttaacaatggttgtttgacatcatttttttcagGATGGCACTTTGATCTACAAG

GTCAAGCTCCGTGGTACCAATTTCCCACCAGATGGACCAGTTATGCAGAAGA

AGACGATGGGATGGGAGGCTTCCACCGAACGATTGTACCCAGAAGATGGAGT

TCTCAAGGGAGACATCAAAATGGCCCTTCGCCTCAAGGACGGAGgtaagtttgatgaa

acggtttcgtcttatatacactaatggtacttttcagGACGTTACCTGGCGGATTTCAAGACCACATA

CAAGGCAAAGAAGCCAGTTCAAATGCCAGGAGCATATAACGTTGACCGCAA

GCTTGATATTACTTCCCATAATGAAGACTACACAGTTGTAGAACAATACGAA

CGATCCGAGGGACGTCATTCGACCGGAGGAATGGACGAGCTGTACAAGTAAa

agtgtctgt

The TAT-5 ATPase hypomorph mutant D244T (PHX2596 tat-5(syb2414[D244T])/+) was generated by CRISPR. Synonymous mutation is labeled in blue.

syb2414: AGATCAATTG**ACCGGT**GAAACTGATT

Wild Type: AGATCAATTG**GATGGA**GAAACTGATT

7.5 Light Microscopy

Embryos were isolated by dissecting adult hermaphrodites on a cover slip in either M9 or egg-salts buffer. Embryos on coverslips were mounted on 4% agarose pad on slides. All fluorescent images were taken with Zeiss Axio Observer 7 inverted microscope with a Plan-Apo 40X 1.4 NA oil objective with Excelitas Technologies X-

Cite 120LED Boost illumination, and a Hamamatsu ORCA-Fusion sCMOS camera controlled by 3i SlideBook6 software. 1 μm step Z-stacks were obtained sequentially for mCherry, and DIC.

Most live images were taken at 20% fluorescent lamp intensity. Live image exposure time and lamp intensity for EV analysis are listed in Table 7.3.

Table 7.3: Imaging parameters for worm strains.

Strain Name	Exposure Time for mCherry	Lamp intensity
WEH434	500ms	10% and 20%
WEH591	500ms	20%
WEH599	500ms	20%
WEH619	500ms	10%
WEH620	500ms	10%
WEH624	500ms	10%
WEH642	400ms	20%
WEH653	400ms	20%
WEH659	400ms	20%
WEH660	400ms	20%
WEH667	400ms	20%
WEH668	400ms	20%
WEH680	400ms	20%

7.6 Time-lapse imaging

Embryos were dissected from gravid adult hermaphrodites and mounted on an 4% agarose pad on slide in M9 buffer. 1 µm step z-stacks were acquired sequentially for DIC, GFP, and mCherry every 30 seconds at room temperature. All images were taken with an AxioObserver 7 inverted microscope with a Plan-Apo 40X 1.4 NA oil objective (Zeiss), X-Cite 120LED Boost illumination (Excelitas Technologies), and ORCA-Fusion sCMOS camera (Hamamatsu) controlled by SlideBook6 software (3i).

7.7 RNA Interference (RNAi)

RNAi was performed by feeding L1 larvae dsRNA from plasmids. RNAi bacteria cultures were grown at 37°C for 6 hours. Gravid adult worms were bleached onto RNAi plates (NGM Lite agar supplemented with Ampicillin, Tetracycline, and Lactose) seeded with 200µl of RNAi culture. Once seeded, worms were bleached on plates and grown at 23˚C for 60-72 hours according to established protocols (Fraser et al., 2000). The following RNAi clones were used in this study: use-1 (mv_Y110A7A.11), pyp-1 (mv_C47E12.4), F01G4.6 (mv_CAA53719), acl-14 (mv_K07B1.5), nbet-1 (sjj2_Y59E9AL.7), ceh-44 (sjj2_Y54F10AM.4a), col-14 (mv_C46A5.4), sdz-27 (mv_R07H5.4), Y41E3.8 (mv_Y41E3.8), F17E9.4 (mv_F17E9.4), ced-1 (mv_Y47H9C.4), F57C2.4 (mv_F57C2.4), C14B1.2 (mv_C14B1.2), C44B7.5 (mv_C44B7.5), F55G1.15 (mv_F55G1.14), B0348.2 (sjj2_B0348.2), LP B0348.2 (this study), Y34F4.2 (sjj2_Y34F4.2), W02D9.6 (mv_W02D9.6), ZK1290.13 (sjj2_ZK1290.13), klc-1 (mv_M7.2), sax-2 (mv_F21H11.1), and klc-2 (mv_CAA82752).

7.8 Plasmid cloning

To remove the second intron in the B0348.2 JA RNAi clone (sjj2_B0348.2), an around the world PCR was performed using Q5 Site-Directed Mutagenesis kit (New England BioLabs). We designed forward primers for B0348.2 third exon and reverse primers for B0348.2 second exon, primer sequence listed in Table 7.4. New B0348.2 plasmids were sequenced. If correct deletion was detected and no other mutations found, the plasmid was transformed into HT115 cells. Competent HT115 cells were thawed on ice and 4µl of B0348.2 LP RNAi bacterial plasmid were added to 50µl HT115 cells. Plasmid and competent cell solution was then incubated on ice for 10 minutes. Then, plasmid and competent cell solution was heat shocked at 42°C for 45 seconds and again incubated on ice for 5 minutes. Next, 250µl LB media was added, and the solution gently shaken and incubated at 37°C for 30 minutes. After incubation, 250µl of LB/plasmid/competent cell solution was spread using a bacterial spreader onto an LB Ampicillin plate and incubated overnight at 37°C. The plate was checked the next day for a successful transformation by scoring single colony growth.

Table 7.4 Primers for deleting second intron in B0348.2 JA RNAi.

Primer name	Sequence	Intended use
B0348.2 exon 2 R	ctggcatttttggcaaaacacctga	In B0348.2 second exon aimed 5' to remove 2nd intron from JA RNAi
B0348.2 exon 3 F	TGC AAT CAA GTG ACA CGT ACT GAG A	In B0348.2 third exon aimed 3' to remove 2nd intron from JA RNAi

7.9 EV Counts

Live images of 3-cell to 15-cell embryos were analyzed for EV puncta in Slidebook6 (3i) by counting individual puncta between the cells and eggshell. EV puncta too close to cells that could not be differentiated from cell plasma membranes with DIC or mCh::coPH::CTPD degron reporter were excluded, likely underestimating the number of EVs, likely undercounting the number of EV puncta as thick clusters or patches of EVs in mutants were counted as 1 or 2 puncta depending on size. Data sets were excluded if embryos were younger than 3-cell stage or older than 15-cell stage.

7.10 EV Counts in the tops of embryos using ImageJ (FIJI)

Analysis of individual EV puncta in the tops of 3-cell to 15-cell embryos in Figure 4.1 was done by Alex Nguyen. EV puncta were counted individually in the top of the embryos using ImageJ (FIJI) “Cell Counter” function. Cell counter was used to mark puncta and keep track of puncta counts. Before analysis the appropriate z-plane at the top of the embryo was selected so only the top of the embryo was in focus while individual cells were not distinguishable. The maximum and minimum brightness settings were

adjusted accordingly to enhance visibility of EVs. Likely undercounting the number of EV puncta as clusters of puncta were estimated according to the average size of EVs for that embryo. Excluded embryos younger than 3 cells and older than 15 cells.

7.11 Scoring LMP-1 puncta

Live images of 2 or 4 cell embryos were analyzed for enlarged or mislocalized LMP-1 positive puncta. Analysis was done by comparison to LMP-1 WT control embryos.

7.12 Scoring midbody remnant and second polar body internalization

Cell stage was identified using DIC. Polar bodies were identified using fluorescent mCh::coPH::CTPD degron reporter. Midbody remnants were labeled and identified using NMY-2:GFP:ZF1 or NMY-2::mCh fluorescent tags. Still and time-lapse images were scored using Slidebook (3i). Internalization was defined as when either the polar body or midbody remnant was fully enclosed by engulfing cells. Polar bodies and midbody remnants sitting between cells were scored as “not internalized”. Midbody remnants were scored from 3-cell to 24-cell, while polar bodies were scored from 3-cell to 15-cell.

7.13 Scoring for Larval Progeny

L4 hermaphrodite larvae were singled onto 24-well plates. Plates were scored for larval progeny 4 days after singling. Scoring larval progeny was assisted by Julia Frondoni.

7.14 Image Manipulation

For clarity, all images were rotated and cropped, and the intensity was adjusted using Adobe Photoshop. AlphaFold2 models were colorized and cropped in PyMol by Ann Wehman (Jumper et al., 2021).

7.15 Statistics

Statistical significance was tested using Student's one-tailed t-test and a Fisher's exact test with Bonferroni correction to adjust for multiple comparisons. The mean ± S.D is depicted in all graphs EV graphs.

References

Abels ER, Breakefield XO. Introduction to Extracellular Vesicles: Biogenesis, RNA Cargo Selection, Content, Release, and Uptake. Cell Mol Neurobiol. 2016 Apr;36(3):301-12. doi: 10.1007/s10571-016-0366-z. Epub 2016 Apr 6. Review. PubMed PMID: 27053351; PubMed Central PMCID: PMC5546313.

Andersen JP, Vestergaard AL, Mikkelsen SA, Mogensen LS, Chalat M, Molday RS. P4-ATPases as Phospholipid Flippases-Structure, Function, and Enigmas. Front Physiol. 2016;7:275. doi: 10.3389/fphys.2016.00275. eCollection 2016. Review. PubMed PMID: 27458383; PubMed Central PMCID: PMC4937031.

Axelsen KB, Palmgren MG. Evolution of substrate specificities in the P-type ATPase superfamily. J Mol Evol. 1998 Jan;46(1):84-101. doi: 10.1007/pl00006286. PubMed PMID: 9419228.

Bai L, Jain BK, You Q, Duan HD, Takar M, Graham TR, Li H. Structural basis of the P4B ATPase lipid flippase activity. Nat Commun. 2021 Oct 13;12(1):5963. doi: 10.1038/s41467-021-26273-0. PubMed PMID: 34645814; PubMed Central PMCID: PMC8514546.

Barbosa S, Pratte D, Schwarz H, Pipkorn R, Singer-Krüger B. Oligomeric Dop1p is part of the endosomal Neo1p-Ysl2p-Arl1p membrane remodeling complex. Traffic. 2010 Aug;11(8):1092-106. doi: 10.1111/j.1600-0854.2010.01079.x. Epub 2010 May 11. PubMed PMID: 20477991.

Beer, K. B. (2021). Identification and characterization of TAT-5 interactors that regulate extracellular vesicle budding. (Doctoral thesis). Universität Würzburg, Würzburg, Germany

Beer KB, Rivas-Castillo J, Kuhn K, Fazeli G, Karmann B, Nance JF, Stigloher C, Wehman AM. Extracellular vesicle budding is inhibited by redundant regulators of TAT-5 flippase localization and phospholipid asymmetry. Proc Natl Acad Sci U S A. 2018 Feb 6;115(6):E1127-E1136. doi: 10.1073/pnas.1714085115. Epub 2018 Jan 24. PubMed PMID: 29367422; PubMed Central PMCID: PMC5819400.

Beer KB, Wehman AM. Mechanisms and functions of extracellular vesicle release in vivo-What we can learn from flies and worms. Cell Adh Migr. 2017 Mar 4;11(2):135-150. doi: 10.1080/19336918.2016.1236899. Epub 2016 Sep 30. Review. PubMed PMID: 27689411; PubMed Central PMCID: PMC5351733.

Beer KB, Fazeli G, Judasova K, Irmisch L, Causemann J, Mansfeld J, Wehman AM. Degron-tagged reporters probe membrane topology and enable the specific labelling of membrane-wrapped structures. Nat Commun. 2019 Aug 2;10(1):3490. doi: 10.1038/s41467-019-11442-z. PubMed PMID: 31375709; PubMed Central PMCID: PMC6677802.

Boulin T, Hobert O. From genes to function: the C. elegans genetic toolbox. Wiley Interdiscip Rev Dev Biol. 2012 Jan-Feb;1(1):114-37. doi: 10.1002/wdev.1. Epub 2011 Nov 28. Review. PubMed PMID: 23801671; PubMed Central PMCID: PMC3694748.

Brenner S. The genetics of Caenorhabditis elegans. Genetics. 1974 May;77(1):71-94. doi: 10.1093/genetics/77.1.71. PubMed PMID: 4366476; PubMed Central PMCID: PMC1213120.

Bryde S, Hennrich H, Verhulst PM, Devaux PF, Lenoir G, Holthuis JC. CDC50 proteins are critical components of the human class-1 P4-ATPase transport machinery. J Biol Chem. 2010 Dec 24;285(52):40562-72. doi: 10.1074/jbc.M110.139543. Epub 2010 Oct 20. PubMed PMID: 20961850; PubMed Central PMCID: PMC3003355.

Castoldi E, Collins PW, Williamson PL, Bevers EM. Compound heterozygosity for 2 novel TMEM16F mutations in a patient with Scott syndrome. Blood. 2011 Apr 21;117(16):4399-400. doi: 10.1182/blood-2011-01-332502. PubMed PMID: 21511967.

Causemann, Jona (2019). Identifying Motifs Involved in the Trafficking of the Essential Lipid Flippase TAT-5 in Caenorhabditis elegans Embryos. (Bachelors Thesis). Universität Würzburg, Würzburg, Germany

Ciardiello C, Cavallini L, Spinelli C, Yang J, Reis-Sobreiro M, de Candia P, Minciacchi VR, Di Vizio D. Focus on Extracellular Vesicles: New Frontiers of Cell-to-Cell Communication in Cancer. Int J Mol Sci. 2016 Feb 6;17(2):175. doi: 10.3390/ijms17020175. Review. PubMed PMID: 26861306; PubMed Central PMCID: PMC4783909.

Colombo M, Raposo G, Théry C. Biogenesis, secretion, and intercellular interactions of exosomes and other extracellular vesicles. Annu Rev Cell Dev Biol. 2014;30:255-89. doi: 10.1146/annurev-cellbio-101512-122326. Epub 2014 Aug 21. Review. PubMed PMID: 25288114.

Coleman JA, Vestergaard AL, Molday RS, Vilsen B, Andersen JP. Critical role of a transmembrane lysine in aminophospholipid transport by mammalian photoreceptor P4-ATPase ATP8A2. Proc Natl Acad Sci U S A. 2012 Jan 31;109(5):1449-54. doi: 10.1073/pnas.1108862109. Epub 2012 Jan 17. PMID: 22307598; PMCID: PMC3277108.

Corrigan L, Redhai S, Leiblich A, Fan SJ, Perera SM, Patel R, Gandy C, Wainwright SM, Morris JF, Hamdy F, Goberdhan DC, Wilson C. BMP-regulated exosomes from Drosophila male reproductive glands reprogram female behavior. J Cell Biol. 2014 Sep 1;206(5):671-88. doi: 10.1083/jcb.201401072. Epub 2014 Aug 25. PubMed PMID: 25154396; PubMed Central PMCID: PMC4151142.

Corsi A.K., Wightman B., and Chalfie M. A Transparent window into biology: A primer on Caenorhabditis elegans (June 18, 2015), WormBook, ed. The C. elegans Research Community, WormBook, doi/10.1895/wormbook.1.177.1, http://www.wormbook.org.

Cui Y, Gao J, He Y, Jiang L. Plant extracellular vesicles. Protoplasma. 2020 Jan;257(1):3-12. doi: 10.1007/s00709-019-01435-6. Epub 2019 Aug 30. Review. PubMed PMID: 31468195.

Darbari E, Zare-Abdollahi D, Alavi A, Rezaei Kanavi M, Feizi S, Hosseini SB, Baradaran-Rafii A, Ahmadieh H, Issazadeh-Navikas S, Elahi E. A mutation in *DOP1B* identified as a probable cause for autosomal recessive Peters anomaly in a consanguineous family. Mol Vis. 2020;26:757-765. eCollection 2020. PubMed PMID: 33273802; PubMed Central PMCID: PMC7700884.

De Palma G, Sallustio F, Schena FP. Clinical Application of Human Urinary Extracellular Vesicles in Kidney and Urologic Diseases. Int J Mol Sci. 2016 Jun 30;17(7). doi: 10.3390/ijms17071043. Review. PubMed PMID: 27376269; PubMed Central PMCID: PMC4964419.

DeRenzo C, Reese KJ, Seydoux G. Exclusion of germ plasm proteins from somatic lineages by cullin-dependent degradation. Nature. 2003 Aug 7;424(6949):685-9. doi: 10.1038/nature01887. Epub 2003 Jul 23. PubMed PMID: 12894212; PubMed Central PMCID: PMC1892537.

Deatherage BL, Cookson BT. Membrane vesicle release in bacteria, eukaryotes, and archaea: a conserved yet underappreciated aspect of microbial life. Infect Immun. 2012 Jun;80(6):1948-57. doi: 10.1128/IAI.06014-11. Epub 2012 Mar 12. Review. PubMed PMID: 22409932; PubMed Central PMCID: PMC3370574.

Dejima K, Hori S, Iwata S, Suehiro Y, Yoshina S, Motohashi T, Mitani S. An Aneuploidy-Free and Structurally Defined Balancer Chromosome Toolkit for Caenorhabditis elegans. Cell Rep. 2018 Jan 2;22(1):232-241. doi: 10.1016/j.celrep.2017.12.024. PubMed PMID: 29298424.

Del Castillo U, Lu W, Winding M, Lakonishok M, Gelfand VI. Pavarotti/MKLP1 regulates microtubule sliding and neurite outgrowth in Drosophila neurons. Curr Biol. 2015 Jan 19;25(2):200-205. doi: 10.1016/j.cub.2014.11.008. Epub 2014 Dec 31. PubMed PMID: 25557664; PubMed Central PMCID: PMC4302008.

Dionne LK, Wang XJ, Prekeris R. Midbody: from cellular junk to regulator of cell polarity and cell fate. Curr Opin Cell Biol. 2015 Aug;35:51-8. doi:

10.1016/j.ceb.2015.04.010. Epub 2015 May 15. Review. PubMed PMID: 25950842; PubMed Central PMCID: PMC4529786.

Edgley, M. L. et al. Genetic balancers (April 6, 2006), *WormBook*, ed. The *C. elegans* Research Community, WormBook, doi/10.1895/wormbook.1.89.1, http://www.wormbook.org.

EL Andaloussi S, Mäger I, Breakefield XO, Wood MJ. Extracellular vesicles: biology and emerging therapeutic opportunities. Nat Rev Drug Discov. 2013 May;12(5):347-57. doi: 10.1038/nrd3978. Epub 2013 Apr 15. Review. PubMed PMID: 23584393.

Emoto K, Kobayashi T, Yamaji A, Aizawa H, Yahara I, Inoue K, Umeda M. Redistribution of phosphatidylethanolamine at the cleavage furrow of dividing cells during cytokinesis. Proc Natl Acad Sci U S A. 1996 Nov 12;93(23):12867-72. doi: 10.1073/pnas.93.23.12867. PubMed PMID: 8917511; PubMed Central PMCID: PMC24012.

Emoto K, Umeda M. An essential role for a membrane lipid in cytokinesis. Regulation of contractile ring disassembly by redistribution of phosphatidylethanolamine. J Cell Biol. 2000 Jun 12;149(6):1215-24. doi: 10.1083/jcb.149.6.1215. PubMed PMID: 10851019; PubMed Central PMCID: PMC2175113.

Emoto K, Toyama-Sorimachi N, Karasuyama H, Inoue K, Umeda M. Exposure of phosphatidylethanolamine on the surface of apoptotic cells. Exp Cell Res. 1997 May 1;232(2):430-4. doi: 10.1006/excr.1997.3521. PubMed PMID: 9168822.

Fabritius AS, Ellefson ML, McNally FJ. Nuclear and spindle positioning during oocyte meiosis. Curr Opin Cell Biol. 2011 Feb;23(1):78-84. doi: 10.1016/j.ceb.2010.07.008. Epub 2010 Aug 11. Review. PubMed PMID: 20708397; PubMed Central PMCID: PMC2994957.

Fazeli G, Trinkwalder M, Irmisch L, Wehman AM. C. elegans midbodies are released, phagocytosed and undergo LC3-dependent degradation independent of macroautophagy. J Cell Sci. 2016 Oct 15;129(20):3721-3731. doi: 10.1242/jcs.190223. Epub 2016 Aug 25. PubMed PMID: 27562069; PubMed Central PMCID: PMC5087666.

Fazeli G, Wehman AM. Safely removing cell debris with LC3-associated phagocytosis. Biol Cell. 2017 Oct;109(10):355-363. doi: 10.1111/boc.201700028. Epub 2017 Aug 25. Review. PubMed PMID: 28755428.

Fazeli G, Stetter M, Lisack JN, Wehman AM. C. elegans Blastomeres Clear the Corpse of the Second Polar Body by LC3-Associated Phagocytosis. Cell Rep. 2018 May 15;23(7):2070-2082. doi: 10.1016/j.celrep.2018.04.043. PubMed PMID: 29768205.

Fazeli G, Beer KB, Geisenhof M, Tröger S, König J, Müller-Reichert T, Wehman AM. Loss of the Major Phosphatidylserine or Phosphatidylethanolamine Flippases

Differentially Affect Phagocytosis. Front Cell Dev Biol. 2020;8:648. doi: 10.3389/fcell.2020.00648. eCollection 2020. PubMed PMID: 32793595; PubMed Central PMCID: PMC7385141.

Feng Z, Zhao Y, Li T, Nie W, Yang X, Wang X, Wu J, Liao J, Zou Y. CATP-8/P5A ATPase Regulates ER Processing of the DMA-1 Receptor for Dendritic Branching. Cell Rep. 2020 Sep 8;32(10):108101. doi: 10.1016/j.celrep.2020.108101. PubMed PMID: 32905774.

Foot N, Henshall T, Kumar S. Ubiquitination and the Regulation of Membrane Proteins. Physiol Rev. 2017 Jan;97(1):253-281. doi: 10.1152/physrev.00012.2016. Review. PubMed PMID: 27932395.

Gallegos ME, Bargmann CI. Mechanosensory neurite termination and tiling depend on SAX-2 and the SAX-1 kinase. Neuron. 2004 Oct 14;44(2):239-49. doi: 10.1016/j.neuron.2004.09.021. PubMed PMID: 15473964.

Gill S, Catchpole R, Forterre P. Extracellular membrane vesicles in the three domains of life and beyond. FEMS Microbiol Rev. 2019 May 1;43(3):273-303. doi: 10.1093/femsre/fuy042. Review. PubMed PMID: 30476045; PubMed Central PMCID: PMC6524685.

Gong J, Jaiswal R, Dalla P, Luk F, Bebawy M. Microparticles in cancer: A review of recent developments and the potential for clinical application. Semin Cell Dev Biol. 2015 Apr;40:35-40. doi: 10.1016/j.semcdb.2015.03.009. Epub 2015 Apr 3. Review. PubMed PMID: 25843775.

Green RA, Kao HL, Audhya A, Arur S, Mayers JR, Fridolfsson HN, Schulman M, Schloissnig S, Niessen S, Laband K, Wang S, Starr DA, Hyman AA, Schedl T, Desai A, Piano F, Gunsalus KC, Oegema K. A high-resolution C. elegans essential gene network based on phenotypic profiling of a complex tissue. Cell. 2011 Apr 29;145(3):470-82. doi: 10.1016/j.cell.2011.03.037. PubMed PMID: 21529718; PubMed Central PMCID: PMC3086541.

Guipponi M, Brunschwig K, Chamoun Z, Scott HS, Shibuya K, Kudoh J, Delezoide AL, El Samadi S, Chettouh Z, Rossier C, Shimizu N, Mueller F, Delabar JM, Antonarakis SE. C21orf5, a novel human chromosome 21 gene, has a Caenorhabditis elegans ortholog (pad-1) required for embryonic patterning. Genomics. 2000 Aug 15;68(1):30-40. doi: 10.1006/geno.2000.6250. PubMed PMID: 10950924.

Henne WM, Buchkovich NJ, Emr SD. The ESCRT pathway. Dev Cell. 2011 Jul 19;21(1):77-91. doi: 10.1016/j.devcel.2011.05.015. Review. PubMed PMID: 21763610.

Henne WM, Stenmark H, Emr SD. Molecular mechanisms of the membrane sculpting ESCRT pathway. Cold Spring Harb Perspect Biol. 2013 Sep 1;5(9). doi:

10.1101/cshperspect.a016766. Review. PubMed PMID: 24003212; PubMed Central PMCID: PMC3753708.

Herrmann IK, Wood MJA, Fuhrmann G. Extracellular vesicles as a next-generation drug delivery platform. Nat Nanotechnol. 2021 Jul;16(7):748-759. doi: 10.1038/s41565-021-00931-2. Epub 2021 Jul 1. Review. PubMed PMID: 34211166.

Hiraizumi M, Yamashita K, Nishizawa T, Nureki O. Cryo-EM structures capture the transport cycle of the P4-ATPase flippase. Science. 2019 Sep 13;365(6458):1149-1155. doi: 10.1126/science.aay3353. Epub 2019 Aug 15. PMID: 31416931.

Hurley JH. ESCRTs are everywhere. EMBO J. 2015 Oct 1;34(19):2398-407. doi: 10.15252/embj.201592484. Epub 2015 Aug 25. Review. PubMed PMID: 26311197; PubMed Central PMCID: PMC4601661.

Hyenne V, Apaydin A, Rodriguez D, Spiegelhalter C, Hoff-Yoessle S, Diem M, Tak S, Lefebvre O, Schwab Y, Goetz JG, Labouesse M. RAL-1 controls multivesicular body biogenesis and exosome secretion. J Cell Biol. 2015 Oct 12;211(1):27-37. doi: 10.1083/jcb.201504136. PubMed PMID: 26459596; PubMed Central PMCID: PMC4602040.

Irie A, Yamamoto K, Miki Y, Murakami M. Phosphatidylethanolamine dynamics are required for osteoclast fusion. Sci Rep. 2017 Apr 24;7:46715. doi: 10.1038/srep46715. PubMed PMID: 28436434; PubMed Central PMCID: PMC5402267.

Jumper J, Evans R, Pritzel A, Green T, Figurnov M, Ronneberger O, Tunyasuvunakool K, Bates R, Žídek A, Potapenko A, Bridgland A, Meyer C, Kohl SAA, Ballard AJ, Cowie A, Romera-Paredes B, Nikolov S, Jain R, Adler J, Back T, Petersen S, Reiman D, Clancy E, Zielinski M, Steinegger M, Pacholska M, Berghammer T, Bodenstein S, Silver D, Vinyals O, Senior AW, Kavukcuoglu K, Kohli P, Hassabis D. Highly accurate protein structure prediction with AlphaFold. Nature. 2021 Aug;596(7873):583-589. doi: 10.1038/s41586-021-03819-2. Epub 2021 Jul 15. PubMed PMID: 34265844; PubMed Central PMCID: PMC8371605.

Kalra H, Drummen GP, Mathivanan S. Focus on Extracellular Vesicles: Introducing the Next Small Big Thing. Int J Mol Sci. 2016 Feb 6;17(2):170. doi: 10.3390/ijms17020170. Review. PubMed PMID: 26861301; PubMed Central PMCID: PMC4783904.

Kapitein LC, Hoogenraad CC. Building the Neuronal Microtubule Cytoskeleton. Neuron. 2015 Aug 5;87(3):492-506. doi: 10.1016/j.neuron.2015.05.046. Review. PubMed PMID: 26247859.

Kume A, Kawase K, Komenoi S, Usuki T, Takeshita E, Sakai H, Sakane F. The Pleckstrin Homology Domain of Diacylglycerol Kinase η Strongly and Selectively Binds to Phosphatidylinositol 4,5-Bisphosphate. J Biol Chem. 2016

Apr 8;291(15):8150-61. doi: 10.1074/jbc.M115.648717. Epub 2016 Feb 17. PubMed PMID: 26887948; PubMed Central PMCID: PMC4825017.

Landschulz WH, Johnson PF, McKnight SL. The leucine zipper: a hypothetical structure common to a new class of DNA binding proteins. Science. 1988 Jun 24;240(4860):1759-64. doi: 10.1126/science.3289117. PubMed PMID: 3289117.

Larson MC, Woodliff JE, Hillery CA, Kearl TJ, Zhao M. Phosphatidylethanolamine is externalized at the surface of microparticles. Biochim Biophys Acta. 2012 Dec;1821(12):1501-7. doi: 10.1016/j.bbalip.2012.08.017. Epub 2012 Aug 30. PubMed PMID: 22960380; PubMed Central PMCID: PMC3809829.

Legrain P, Selig L. Genome-wide protein interaction maps using two-hybrid systems. FEBS Lett. 2000 Aug 25;480(1):32-6. doi: 10.1016/s0014-5793(00)01774-9. Review. PubMed PMID: 10967325.

Leventis PA, Grinstein S. The distribution and function of phosphatidylserine in cellular membranes. Annu Rev Biophys. 2010;39:407-27. doi: 10.1146/annurev.biophys.093008.131234. Review. PubMed PMID: 20192774.

Li R, Albertini DF. The road to maturation: somatic cell interaction and self-organization of the mammalian oocyte. Nat Rev Mol Cell Biol. 2013 Mar;14(3):141-52. doi: 10.1038/nrm3531. Review. PubMed PMID: 23429793.

Lin S, Liu M, Mozgova OI, Yu W, Baas PW. Mitotic motors coregulate microtubule patterns in axons and dendrites. J Neurosci. 2012 Oct 3;32(40):14033-49. doi: 10.1523/JNEUROSCI.3070-12.2012. PubMed PMID: 23035110; PubMed Central PMCID: PMC3482493.

Liégeois S, Benedetto A, Garnier JM, Schwab Y, Labouesse M. The V0-ATPase mediates apical secretion of exosomes containing Hedgehog-related proteins in Caenorhabditis elegans. J Cell Biol. 2006 Jun 19;173(6):949-61. doi: 10.1083/jcb.200511072. PubMed PMID: 16785323; PubMed Central PMCID: PMC2063919.

Lu W, Fox P, Lakonishok M, Davidson MW, Gelfand VI. Initial neurite outgrowth in Drosophila neurons is driven by kinesin-powered microtubule sliding. Curr Biol. 2013 Jun 3;23(11):1018-23. doi: 10.1016/j.cub.2013.04.050. Epub 2013 May 23. PubMed PMID: 23707427; PubMed Central PMCID: PMC3676710.

Lyssenko NN, Miteva Y, Gilroy S, Hanna-Rose W, Schlegel RA. An unexpectedly high degree of specialization and a widespread involvement in sterol metabolism among the C. elegans putative aminophospholipid translocases. BMC Dev Biol. 2008 Oct 2;8:96. doi: 10.1186/1471-213X-8-96. PubMed PMID: 18831765; PubMed Central PMCID: PMC2572054.

López-Marqués RL, Gourdon P, Günther Pomorski T, Palmgren M. The transport mechanism of P4 ATPase lipid flippases. Biochem J. 2020 Oct 16;477(19):3769-3790. doi: 10.1042/BCJ20200249. Review. PubMed PMID: 33045059.

Mahajan D, Tie HC, Chen B, Lu L. Dopey1-Mon2 complex binds to dual-lipids and recruits kinesin-1 for membrane trafficking. Nat Commun. 2019 Jul 19;10(1):3218. doi: 10.1038/s41467-019-11056-5. PubMed PMID: 31324769; PubMed Central PMCID: PMC6642134.

Mathieu M, Martin-Jaular L, Lavieu G, Théry C. Specificities of secretion and uptake of exosomes and other extracellular vesicles for cell-to-cell communication. Nat Cell Biol. 2019 Jan;21(1):9-17. doi: 10.1038/s41556-018-0250-9. Epub 2019 Jan 2. Review. PubMed PMID: 30602770.

McKenna MJ, Sim SI, Ordureau A, Wei L, Harper JW, Shao S, Park E. The endoplasmic reticulum P5A-ATPase is a transmembrane helix dislocase. Science. 2020 Sep 25;369(6511). doi: 10.1126/science.abc5809. PubMed PMID: 32973005; PubMed Central PMCID: PMC8053355.

Molière A, Beer KB, Wehman AM. Dopey proteins are essential but overlooked regulators of membrane trafficking. J Cell Sci. 2022 Apr 1;135(7). doi: 10.1242/jcs.259628. Epub 2022 Apr 7. Review. PubMed PMID: 35388894.

Nabhan JF, Hu R, Oh RS, Cohen SN, Lu Q. Formation and release of arrestin domain-containing protein 1-mediated microvesicles (ARMMs) at plasma membrane by recruitment of TSG101 protein. Proc Natl Acad Sci U S A. 2012 Mar 13;109(11):4146-51. doi: 10.1073/pnas.1200448109. Epub 2012 Feb 6. PubMed PMID: 22315426; PubMed Central PMCID: PMC3306724.

Nishi Y, Lin R. DYRK2 and GSK-3 phosphorylate and promote the timely degradation of OMA-1, a key regulator of the oocyte-to-embryo transition in C. elegans. Dev Biol. 2005 Dec 1;288(1):139-49. doi: 10.1016/j.ydbio.2005.09.053. Epub 2005 Nov 11. PubMed PMID: 16289132.

Norkett R, Del Castillo U, Lu W, Gelfand VI. Ser/Thr kinase Trc controls neurite outgrowth in *Drosophila* by modulating microtubule-microtubule sliding. Elife. 2020 Feb 5;9. doi: 10.7554/eLife.52009. PubMed PMID: 32022690; PubMed Central PMCID: PMC7021487.

Ohno S, Drummen GP, Kuroda M. Focus on Extracellular Vesicles: Development of Extracellular Vesicle-Based Therapeutic Systems. Int J Mol Sci. 2016 Feb 6;17(2):172. doi: 10.3390/ijms17020172. Review. PubMed PMID: 26861303; PubMed Central PMCID: PMC4783906.

Okamoto A, Yabuta N, Mukai S, Torigata K, Nojima H. Phosphorylation of CHO1 by Lats1/2 regulates the centrosomal activation of LIMK1 during cytokinesis. Cell Cycle. 2015;14(10):1568-82. doi: 10.1080/15384101.2015.1026489. PubMed PMID: 25786116; PubMed Central PMCID: PMC4613183.

Ou G, Gentili C, Gönczy P. Stereotyped distribution of midbody remnants in early C. elegans embryos requires cell death genes and is dispensable for development.

Cell Res. 2014 Feb;24(2):251-3. doi: 10.1038/cr.2013.140. Epub 2013 Oct 15. PubMed PMID: 24126714; PubMed Central PMCID: PMC3916897.

Paix A, Wang Y, Smith HE, Lee CY, Calidas D, Lu T, Smith J, Schmidt H, Krause MW, Seydoux G. Scalable and versatile genome editing using linear DNAs with microhomology to Cas9 Sites in Caenorhabditis elegans. Genetics. 2014 Dec;198(4):1347-56. doi: 10.1534/genetics.114.170423. Epub 2014 Sep 23. PubMed PMID: 25249454; PubMed Central PMCID: PMC4256755.

Palmgren M, Østerberg JT, Nintemann SJ, Poulsen LR, López-Marqués RL. Evolution and a revised nomenclature of P4 ATPases, a eukaryotic family of lipid flippases. Biochim Biophys Acta Biomembr. 2019 Jun 1;1861(6):1135-1151. doi: 10.1016/j.bbamem.2019.02.006. Epub 2019 Feb 23. PubMed PMID: 30802428.

Palmgren MG, Nissen P. P-type ATPases. Annu Rev Biophys. 2011;40:243-66. doi: 10.1146/annurev.biophys.093008.131331. Review. PubMed PMID: 21351879.

Pascon RC, Miller BL. Morphogenesis in Aspergillus nidulans requires Dopey (DopA), a member of a novel family of leucine zipper-like proteins conserved from yeast to humans. Mol Microbiol. 2000 Jun;36(6):1250-64. doi: 10.1046/j.1365-2958.2000.01950.x. PubMed PMID: 10931277.

Praitis V, Casey E, Collar D, Austin J. Creation of low-copy integrated transgenic lines in Caenorhabditis elegans. Genetics. 2001 Mar;157(3):1217-26. doi: 10.1093/genetics/157.3.1217. PMID: 11238406; PMCID: PMC1461581.

Rachidi M, Delezoide AL, Delabar JM, Lopes C. A quantitative assessment of gene expression (QAGE) reveals differential overexpression of DOPEY2, a candidate gene for mental retardation, in Down syndrome brain regions. Int J Dev Neurosci. 2009 Jun;27(4):393-8. doi: 10.1016/j.ijdevneu.2009.02.001. Epub 2009 Feb 13. PubMed PMID: 19460634.

Rees DC, Johnson E, Lewinson O. ABC transporters: the power to change. Nat Rev Mol Cell Biol. 2009 Mar;10(3):218-27. doi: 10.1038/nrm2646. Review. PubMed PMID: 19234479; PubMed Central PMCID: PMC2830722.

Sahu SK, Gummadi SN, Manoj N, Aradhyam GK. Phospholipid scramblases: an overview. Arch Biochem Biophys. 2007 Jun 1;462(1):103-14. doi: 10.1016/j.abb.2007.04.002. Epub 2007 Apr 17. Review. PubMed PMID: 17481571.

Saito K, Fujimura-Kamada K, Furuta N, Kato U, Umeda M, Tanaka K. Cdc50p, a protein required for polarized growth, associates with the Drs2p P-type ATPase implicated in phospholipid translocation in Saccharomyces cerevisiae. Mol Biol Cell. 2004 Jul;15(7):3418-32. doi: 10.1091/mbc.e03-11-0829. Epub 2004 Apr 16. PubMed PMID: 15090616; PubMed Central PMCID: PMC452594.

Schwechheimer C, Kuehn MJ. Outer-membrane vesicles from Gram-negative bacteria: biogenesis and functions. Nat Rev Microbiol. 2015 Oct;13(10):605-19. doi:

10.1038/nrmicro3525. Review. PubMed PMID: 26373371; PubMed Central PMCID: PMC5308417.

Shelton CA, Carter JC, Ellis GC, Bowerman B. The nonmuscle myosin regulatory light chain gene mlc-4 is required for cytokinesis, anterior-posterior polarity, and body morphology during Caenorhabditis elegans embryogenesis. J Cell Biol. 1999 Jul 26;146(2):439-51. doi: 10.1083/jcb.146.2.439. PubMed PMID: 10427096; PubMed Central PMCID: PMC3206578.

Shin HW, Takatsu H. Substrates of P4-ATPases: beyond aminophospholipids (phosphatidylserine and phosphatidylethanolamine). FASEB J. 2019 Mar;33(3):3087-3096. doi: 10.1096/fj.201801873R. Epub 2018 Dec 3. Review. PubMed PMID: 30509129.

Stone MC, Nguyen MM, Tao J, Allender DL, Rolls MM. Global up-regulation of microtubule dynamics and polarity reversal during regeneration of an axon from a dendrite. Mol Biol Cell. 2010 Mar 1;21(5):767-77. doi: 10.1091/mbc.e09-11-0967. Epub 2010 Jan 6. PubMed PMID: 20053676; PubMed Central PMCID: PMC2828963.

Sulston JE, Schierenberg E, White JG, Thomson JN. The embryonic cell lineage of the nematode Caenorhabditis elegans. Dev Biol. 1983 Nov;100(1):64-119. doi: 10.1016/0012-1606(83)90201-4. PubMed PMID: 6684600.

Suzuki J, Umeda M, Sims PJ, Nagata S. Calcium-dependent phospholipid scrambling by TMEM16F. Nature. 2010 Dec 9;468(7325):834-8. doi: 10.1038/nature09583. Epub 2010 Nov 24. PubMed PMID: 21107324.

Tamai K, Tanaka N, Nakano T, Kakazu E, Kondo Y, Inoue J, Shiina M, Fukushima K, Hoshino T, Sano K, Ueno Y, Shimosegawa T, Sugamura K. Exosome secretion of dendritic cells is regulated by Hrs, an ESCRT-0 protein. Biochem Biophys Res Commun. 2010 Aug 27;399(3):384-90. doi: 10.1016/j.bbrc.2010.07.083. Epub 2010 Jul 29. PubMed PMID: 20673754.

Timcenko M, Lyons JA, Januliene D, Ulstrup JJ, Dieudonné T, Montigny C, Ash MR, Karlsen JL, Boesen T, Kühlbrandt W, Lenoir G, Moeller A, Nissen P. Structure and autoregulation of a P4-ATPase lipid flippase. Nature. 2019 Jul;571(7765):366-370. doi: 10.1038/s41586-019-1344-7. Epub 2019 Jun 26. PubMed PMID: 31243363.

Torrano V, Royo F, Peinado H, Loizaga-Iriarte A, Unda M, Falcón-Perez JM, Carracedo A. Vesicle-MaNiA: extracellular vesicles in liquid biopsy and cancer. Curr Opin Pharmacol. 2016 Aug;29:47-53. doi: 10.1016/j.coph.2016.06.003. Epub 2016 Jun 28. Review. PubMed PMID: 27366992; PubMed Central PMCID: PMC4992611.

Ward S, Carrel JS. Fertilization and sperm competition in the nematode Caenorhabditis elegans. Dev Biol. 1979 Dec;73(2):304-21. doi: 10.1016/0012-1606(79)90069-1. PubMed PMID: 499670.

Wehman AM, Poggioli C, Schweinsberg P, Grant BD, Nance J. The P4-ATPase TAT-5 inhibits the budding of extracellular vesicles in C. elegans embryos. Curr Biol. 2011 Dec 6;21(23):1951-9. doi: 10.1016/j.cub.2011.10.040. Epub 2011 Nov 17. PubMed PMID: 22100064; PubMed Central PMCID: PMC3237752.

Winding M, Kelliher MT, Lu W, Wildonger J, Gelfand VI. Role of kinesin-1-based microtubule sliding in Drosophila nervous system development. Proc Natl Acad Sci U S A. 2016 Aug 23;113(34):E4985-94. doi: 10.1073/pnas.1522416113. Epub 2016 Aug 10. PubMed PMID: 27512046; PubMed Central PMCID: PMC5003282.

Yang HY, Mains PE, McNally FJ. Kinesin-1 mediates translocation of the meiotic spindle to the oocyte cortex through KCA-1, a novel cargo adapter. J Cell Biol. 2005 May 9;169(3):447-57. doi: 10.1083/jcb.200411132. PubMed PMID: 15883196; PubMed Central PMCID: PMC2171918.

Zallen JA, Kirch SA, Bargmann CI. Genes required for axon pathfinding and extension in the C. elegans nerve ring. Development. 1999 Aug;126(16):3679-92. doi: 10.1242/dev.126.16.3679. PubMed PMID: 10409513.

Zallen JA, Peckol EL, Tobin DM, Bargmann CI. Neuronal cell shape and neurite initiation are regulated by the Ndr kinase SAX-1, a member of the Orb6/COT-1/warts serine/threonine kinase family. Mol Biol Cell. 2000 Sep;11(9):3177-90. doi: 10.1091/mbc.11.9.3177. PubMed PMID: 10982409; PubMed Central PMCID: PMC14984.

Zhao SB, Dean N, Gao XD, Fujita M. MON2 Guides Wntless Transport to the Golgi through Recycling Endosomes. Cell Struct Funct. 2020 Jun 13;45(1):77-92. doi: 10.1247/csf.20012. Epub 2020 May 12. PubMed PMID: 32404555.

Zwaal RF, Comfurius P, Bevers EM. Surface exposure of phosphatidylserine in pathological cells. Cell Mol Life Sci. 2005 May;62(9):971-88. doi: 10.1007/s00018-005-4527-3. Review. PubMed PMID: 15761668.

van Niel G, D'Angelo G, Raposo G. Shedding light on the cell biology of extracellular vesicles. Nat Rev Mol Cell Biol. 2018 Apr;19(4):213-228. doi: 10.1038/nrm.2017.125. Epub 2018 Jan 17. Review. PubMed PMID: 29339798.

van der Mark VA, Elferink RP, Paulusma CC. P4 ATPases: flippases in health and disease. Int J Mol Sci. 2013 Apr 11;14(4):7897-922. doi: 10.3390/ijms14047897. Review. PubMed PMID: 23579954; PubMed Central PMCID: PMC3645723.

van der Velden LM, Wichers CG, van Breevoort AE, Coleman JA, Molday RS, Berger R, Klomp LW, van de Graaf SF. Heteromeric interactions required for abundance and subcellular localization of human CDC50 proteins and class 1 P4-ATPases. J Biol Chem. 2010 Dec 17;285(51):40088-96. doi: 10.1074/jbc.M110.139006. Epub 2010 Oct 14. PubMed PMID: 20947505; PubMed Central PMCID: PMC3000991.